Modeling Hereditary Diffuse Leukoencephalopathy with Axonal Spheroids using microglia-sufficient brain organoids

Wei Jie Wong[1,*], Yi Wen Zhu[1,*], Hai Ting Wang[1], Jia Wen Qian[1], Ziyi Li[1], Song Li[1], Zhao Yuan Liu[1], Wei Guo[1], Shuang Yan Zhang[1], Bing Su[1], Fang Ping He[2], Kang Wang[2,], and Florent Ginhoux[1,3,4,5,6,#]

[1]Shanghai Institute of Immunology, Department of Immunology and Microbiology, Shanghai Jiao Tong University School of Medicine, Shanghai 200025, China
[2]Department of Neurology, First Affiliated Hospital of Zhejiang University, Hangzhou 310003, China
[3]Singapore Immunology Network, Agency for Science, Technology and Research, 138648, Singapore
[4]Department of Microbiology and Immunology, Yong Loo Lin School of Medicine, National University of Singapore, 117545, Singapore
[5]INSERM U1015, Gustave Roussy Cancer Campus, Villejuif 94800, France
[6]Translational Immunology Institute, SingHealth Duke-NUS Academic Medical Centre, Singapore 169856, Singapore

*Equal Contribution
#Lead contact, Correspondence: (F.G., florent_ginhoux@immunol.a-star.edu.sg)
Co-correspondence: (K.W., fcwangk1@zju.edu.cn)

Abstract

Hereditary diffuse leukoencephalopathy with axonal spheroids (HDLS) is a rare, fatal, adult-onset neurodegenerative disease that is most often caused by mutations affecting the Colony Stimulating factor-1 Receptor (CSF-1R). To understand how CSF-1R-mutation affects human microglia – the specialized brain-resident macrophages of the central nervous system – and the downstream consequences for neuronal cells, we used a macrophage and forebrain organoid co-culture system based on induced pluripotent stem cells generated from two patients with HDLS, with *CSF-1R* gene-corrected isogenic organoids as controls. Macrophages derived from iPSC (iMacs) of patients exhibited a metabolic shift towards the glycolytic pathway and reduced CSF-1 sensitivity, which was associated with higher levels of IL-1β production and an activated inflammatory phenotype. Single-cell RNA sequencing revealed that iMacs adopt a reactive state that leads to impaired regulation of neuronal cell populations in organoid cultures, thereby identifying microglial dysregulation and specifically IL-1β production as key contributors to the degenerative neuro-environment in HDLS.

Key words:

HDLS, CSF-1R, neurodegenerative disease, iPSC-induced primitive macrophages, iMac, forebrain organoid, co-culture, IL-1beta

Introduction

Hereditary diffused leukoencephalopathy with axonal spheroids (HDLS) – also known as adult-onset leukodystrophy with axonal spheroids and pigmented glia (ALSP), is a rare, inherited, autosomal dominant, neurodegenerative disease that is characterized by patchy axonal swellings (spheroids) and demyelination that result in the alteration of the white matter of the brain (1). Although detailed epidemiological data are lacking, in 2021, it was estimated that approximately a quarter of a million people globally are affected by the condition (2); yet our understanding of the pathogenesis of the disease is limited, and there is no cure or even effective treatment.

For more than a decade, we have known that HDLS is caused by mutations affecting the colony-stimulating factor-1 receptor (CSF-1R) (3) which most often occur in the tyrosine kinase domain (TKD) (4), and lead to reduced auto-phosphorylation in response to CSF-1, which results in impaired downstream signaling (4, 5). These mutations most profoundly affect microglia (6), the specialized brain-resident macrophages that play critical roles in brain development and homeostasis (7, 8) as well as in a wide range of neuroinflammatory and neurodegenerative diseases (9). Patients with HDLS have few, small, microglia that are distributed abnormally within the neocortex and that express low levels of the homeostatic marker P2RY12 and high levels of the inflammatory marker CD68, compared to healthy controls (10-12).

Studies aiming to understand the pathophysiology of HDLS have used various approaches.

Rodent models have been generated, but do not faithfully recapitulate the disease phenotype in humans: the earliest haplo-insufficient Csf-1r$^{+/-}$ mice model exhibited microgliosis within brain regions (13), but this was not recapitulated in a later Csf-1r knockout rat model (14); while a subsequent orthologous mouse model has phenocopied the reduced microglia density seen in patients with HDLS but does not exhibit brain pathology (15). A zebrafish model of HDLS similarly saw reduced microglia during brain development (16), but does not offer the opportunity to study pathology associated with adult-onset neurodegenerative diseases (17). To overcome these species-specific limitations, in this study we generated human induced pluripotent stem cell (iPSC) -derived macrophages from patients with HDLS and used them to create microglia-sufficient autologous brain organoids (18) in which we characterized the effects of naturally occurring *CSF-1R* mutation on microglial function. By comparing iPSC-derived macrophages to genetically corrected macrophages from the same patients, we uncovered evidence of significant transcriptional and metabolic reprogramming that was associated with profound changes to neuronal regulation by these cells, indicative of the likely mechanistic links between microglial dysfunction and HDLS.

RESULTS

Generation and characterization of iPSC lines from patients with HDLS

We first isolated dermal fibroblasts from skin biopsies taken from two patients with HDLS and confirmed mutations in the TDK region of the *CSF-1R* gene (HD1, HD2; clinical characteristics shown in Supplemental Table 1) then cultured them for approximately four

weeks before reprogramming into induced pluripotent stem cells (iPSCs) (**Fig 1A**). Four to five weeks post-transfection, we observed iPSC-like colonies emerging (**Supp Fig 1B**), and 7-10 days later, we selected those clones that were proliferating and displayed typical iPSC morphology (**Fig 1C**). We confirmed successful reprogramming by visualization of pluripotency markers including SOX2 and OCT4 (nuclear markers), and TRA-1-60 and SSEA-4 (intracellular marker), by immunofluorescence (**Fig 1D**). We also confirmed that these clones had normal karyotype (**Fig 1E**) and termed them Mut HD1 and Mut HD2. One clone per cell line was used for further analysis. We then generated isogenic from Mut HD1 and Mut HD2 iPSC cell lines which we termed IsoHD1 and IsoHD2 respectively, as controls (see Methods). Clones that were karyotypically normal were used for downstream experiments alongside their mutant counterparts (**Fig 1B**), with no off-target events identified (**Supp Fig 1C**). Collectively, HDLS iPSC and their corresponding isogenic iPSC controls were successfully generated from two patients with HDLS (HD1 and HD2).

Generation and characterization of patient iPSC-derived macrophages

We next sought to differentiate primitive microglia-like macrophages from patient-derived iPSC cell lines (iMacs) using our serum-free protocol that faithfully recapitulates the generation of *in vivo* microglial progenitor cells (19). Briefly, iPSCs were initially inducted towards the mesodermal lineage before being differentiated into hemangioblast-like cells with the potential to differentiate into both endothelial and hematopoietic progenitors - the latter emerging as free-floating cells as early as day six after seeding -

which we collected and then terminally differentiated into iMacs by the addition of CSF-1 (**Fig 2A**). Although HDLS mutation downregulates the sensitivity of CSF-1R to its ligand (5), we were able to successfully generate iMacs using this protocol: the yield of iMacs from iPSC varied between cultures (**Fig 2B**), but flow cytometry confirmed their consistent macrophage-like phenotype, with abundant expression of CD45 and CD14 (**Fig 2C**), and Giemsa staining showed that iMacs exhibited comparable morphology between donors (**Fig 2D**). Functionally, all iMac cultures were equally able to take up PE-labelled beads that were detectable within their cell bodies (**Fig 2D**); flow cytometry confirmed that the level of actin-dependent phagocytosis of pHrodo beads was comparable among CD45-expressing cells from all cultures (**Fig 2E**). Collectively, these data show that iMacs generated from HDLS donor-derived iPSC adopted the typical morphology, phenotype and functions associated with macrophages.

The mutations associated with HDLS downregulate the sensitivity of CSF-1R to its ligand CSF-1, but to different extents depending on the mutation site (5). We therefore compared the survival of our mutant and isogenic cells lines from both patients during culture with CSF-1. As expected, even with high concentrations of CSF-1, relatively few mutant cells survived across seven days of culture; by contrast, even low CSF-1 levels allowed significantly more isogenic cells to survive (**Fig 2F).**

In summary, we generated iMacs from iPSC of patients with HDLS and their respective isogenic controls that exhibit typical macrophage morphology, phenotype, and phagocytic

capabilities.

Mutant and isogenic control iMacs have distinct gene expression profiles

Although iMacs derived from patients with HDLS exhibited core macrophage features, we wanted to more fully understand the impact of *CSF-1R* mutation on these cells. We first characterized their gene expression profile using bulk RNA-seq and compared it to that of their respective *CSF-1R*-restored isogenic iMac cultures.

Principal component analysis (PCA) showed that patterns of gene expression differed markedly between mutant and isogenic iMacs. Among cell cultures from HD1, mutant iMacs exhibited patterns of gene expression consistent with a more reactive state compared to isogenic *CSF-1R*-restored HD1: HD1 Mut had higher expression of genes involved in pathways related to proliferation (IGF2, MYBL2, STAT1, INCEP, TGFA) and the defense response to virus (IFI27, IFI44L, STAT1, MX1, IFIT3); while Iso HD1 iMacs expressed high levels of genes involved in chemokine-related responses and signaling pathways (CXCL2, ADAM8, CCL31L, CCL5,), as well as leukocyte migration and chemotaxis (CXCL3, CCL13, CCL2, E5AR1, C3AR1) (**Fig 3A-C**). We observed a similar transcriptomic profile in HD2-derived iMacs: HD2 Mut showed up-regulated gene expression for the defensive response to virus, while isogenic HD2 iMacs exhibited high expression levels of genes involved in leukocyte migration and chemotaxis (**Fig 3D-F**). These data are in line with previous reports suggesting that macrophages from patients with HDLS adopt an inflammatory phenotype with increased expression of the immunoreactive markers CD68 and CD163 (10, 12). Additionally, an upregulation of the

immature myeloid cell marker MPO (20), and a reduced expression of mature macrophage marker MARCO (21) was observed within mutant iMac of both cell lines. Taken together, iMac cultures derived from patients with HDLS exhibited transcriptomic profiles consistent with upregulated inflammatory gene expression as a result of impeded CSF-1R function.

Mutant and isogenic control iMacs have distinct metabolic profiles

Studies have shown that activated macrophages often undergo metabolic reprogramming to fulfil the energetic needs of demanding biochemical processes (22, 23); alongside, we know that energy metabolism, as well as metabolic cell features, plays an important role in mediating macrophage function and plasticity (24). Therefore, we next compared the cellular metabolic profiles of patient-derived *CSF-1R* mutant and isogenic *CSF-1R*-restored iMacs.

We first assessed glycolysis by measuring the extracellular acidification rate (ECAR) in the presence of specific modulators (glucose, oligomycin, 2-deoxy-glucose) that were added sequentially to the cell cultures to reveal various aspects of the metabolic pathway (see Methods): this showed that *CSF-1R*-mutant iMacs from both HD1 and HD2 had a significant overall increase in glycolytic function (**Fig 3G and 3O**). Although the magnitude of the difference between iMac HD1 and HD2 and their respective *CSF-1R*-restored counterparts varied, in both cases, *CSF-1R* mutation was associated with significantly increased glycolytic capacity and glycolytic reserve.

Next, we determined the functional metabolic profile of mitochondrial respiration by measuring real-time changes in the extracellular oxygen consumption rate (OCR) during sequential treatment of cells with oligomycin, carbonyl cynide p-trifluoromethoxyphenylhydrazone (FCCP) and a combination of rotenone and antimycin A. As before, although the magnitude of effect was less for cells from HD1, both sets of iMacs showed a similar trend towards higher OCR values, and greater capacity for basal respiration, ATP production, and maximal respiratory capacity in the presence of mutated *CSF-1R* in the case of HD2 Mut cells, these differences achieved statistical significance across all three bioenergetic parameters.

Taken together, these results indicate that the absence of fully functional CSF-1R in cells from HD1 and HD2 is associated with an upregulated glycolytic metabolic profile, which is cells from HD2 is clearly accompanied by a higher mitochondrial oxidative phosphorylation rate. This suggests that macrophages from patients with HDLS have an altered metabolic profile that correlates with their higher activation status and could contribute to disease pathology.

HDLS iMacs upregulate IL-1β when exposed to apoptotic neuronal cells

Our data suggest that mutant iMacs have dysregulated transcriptomic and metabolic profiles, suggestive of an active inflammatory state. To better understand how this would be expressed in the context of their functions in the brain, we mimicked a need for apoptotic cell clearance by incubating iMacs from patients with HDLS with UV-irradiated

neuronal SH-SY5Y cells (**Supp Fig 2A**). Both iMac lines (*CSF-1R* mutant and isogenic) from both patients effectively phagocytosed apoptotic but not control, non-UV-irradiated, SH-SY5Y cells, in an actin-dependent manner (**Supp Fig 2B**).

We then measured the expression of genes encoding pro- (IFN-g, TNF-α, IL-1β, IL-6, IL-18) and anti- (IL-10, IL-12, TGF-β) inflammatory cytokines following incubation of iMacs with UV-irradiated or non-irradiated SH-SY5Y cells, or without any SH-SY5Y cells, for eight hours. We observed a significant and specific increase in IL-1β transcription in *CSF-1R* mutated iMacs from both HD1 and HD2 when exposed to apoptotic cells, compared with their isogenic counterparts. Among the anti-inflammatory cytokines, Mut HD2 cells exhibited significantly increased transcription of the gene encoding TGF-β when cocultured with UV-treated cells, alongside high baseline levels of IL-12 and TGF-β in control cultures compared to isogenic HD2 iMacs. Interestingly, all *CSF-1R* mutant iMac groups had higher levels of transcription of most pro-inflammatory cytokines at baseline, consistent with their activated/reactive transcriptional profile, than did their *CSF-1R*-restored counterparts (**Fig 4A-B**).

Collectively, all iMacs exhibited the ability to specifically phagocytose apoptotic cells, but in the absence of a fully functional CSF-1R, this led to high levels of IL-1β transcription, which reflected a general propensity towards the transcription of pro-inflammatory cytokine genes, even in the absence of overt stimulation. Importantly, restoration of *CSF-1R* via gene editing was sufficient to reverse this inflammatory phenotype.

iMacs differentiate into microglia-like cells (iMicro) in a coculture with forebrain organoid

During HDLS, patients typically exhibit degeneration of the frontal lobes of the brain, which contributes to the deficit and decline in cognitive ability, changes to personality and behavior, and dysfunctional motor, social, and language skills (25, 26). Therefore, we next generated iPSC-derived forebrain organoids including autologous iMacs from patients with HDLS to better understand their potential role in the brain.

To better understand how diseased or non-diseased macrophages affect the developing brain, we first generated forebrain organoids from the isogenic cell line variant of the respective donor's iPSC (see Methods). After 31 days, organoids were harvested (**Supp Fig 3A**) and co-cultured for seven days with isogenic or mutant iMacs that had been generated in parallel (**Fig 5A**). At this point, each organoid was removed from its coculture and cultured individually for 16 more days (**Fig 5B**).

We then applied 3D imaging of forebrain organoids to assess their morphology and the distribution/differentiation of the iMacs. This showed that iMacs expressing the microglial marker IBA-1, were mostly located on the surface of the organoids (**Fig 5C**). We also labelled organoids for NESTIN (a neuronal cell marker) and SOX2 (expressed by neuronal progenitor cells (NPCs). In all of the organoids, neural epithelial rosettes were present, consisting mostly of $SOX2^{+}$ NPCs (**Supp Fig 3B**); these structures indicate favorable organoid growth as they demonstrate proper lineage progression leading to forebrain region identity (27) Importantly, organoids to which we did not add iMacs did

not contain any IBA-1^{+} cells (**Supp Fig 3C**); this was as expected from our previous work (18), but was in contrast to previous studies that reported innately-derived microglia in mesodermal-lineage-containing cerebral organoids (27, 28).

Next, we characterized the different cell populations within organoids after 23 days of coculture and compared iMacs before and after co-culture. After organoid dissociation, cells were labelled with antibodies to differentiate neurons (CD45^{-}/CD184^{-}/CD44^{-}/CD15^{lo}/CD24^{+}), NPCs (CD45^{-}/CD184^{+}/CD271^{-}/CD44^{-}/CD24^{+}) and iMacs (CD45^{+}) before undergoing sorting (**Fig 5D**) followed by bulk-RNA sequencing. During the course of the work, sufficient iMicro numbers for downstream analysis were only generated from coculture with mutant iMacs for HD1 and isogenic iMacs for HD2 respectively. Compared to Day 31 non-co-cultured iMacs, HD1 iMacs after co-culture had profoundly altered their gene expression (**Fig 5E**), with the upregulated DEGs showing an increase in various pathways that are characteristic of microglial functions in the brain such as central nervous system and brain development (CNTN1, ZIC2, EFNA2, GLI3), synapse organization, synapse and neuron organization and development (SLC1A1, DGKB, TRIM67), as well as neurogenesis (CHD11, ADCYAP1) (**Fig 5F-G**).

Likewise, for HD2 iMacs, PCA also suggested that their patterns of gene expression were markedly different between cocultured and non-cocultured populations (**Fig 5H**), while GO analysis of the upregulated DEGs revealed an increase in various pathways linked with typical microglial functions in the brain such as glial cell differentiation and

gliogenesis (CLU, MDK, CXCR4, RELN, TMEM98, TUBA1A), axonal development (UCHL1, MAP1B, CRABP2, TUBB2B, LGI1) as well as forebrain development (TUBB2B, MDK, CXCR4, RELN, LHX2) (**Fig 5I-J**). This shows that iMacs undergoing coculture with forebrain organoids have differentiated to a certain extent, into microglia-like cells.

Co-culture results in impaired regulation of neurons within organoids

Microglia not only act as sentinel cells, but are also important contributors to neuroplasticity and neurogenesis in the developing brain that ultimately help shape the brain circuitry (29). Part of this role requires microglia to regulate the population of NPCs and neurons during the unrestrained, highly proliferative phase of early brain development (30, 31); therefore, we next asked whether the microglia-like cells from our iMac-forebrain organoids were also capable of regulating neurogenesis *in vitro*.

As such, we sought to compare the size of the organoids, as well as the individual major cell population in each organoid, for both variants between isogenic organoids that did not undergo co-culture, and those that underwent 23 days of co-culture by comparing their area before and after co-culture. Co-culture of HD1 saw a slight reduction in the organoid size among both co-culture parameters before and after co-culture. However, comparison of the organoid size on coculture Day 23 only, saw the isogenic control parameter as the only group that had a reduction in organoid size when compared to the organoid-only control (**Fig 6A**). On the contrary, HD2 displayed no significance in organoid size reduction even after co-culture (**Fig 6B**).

Subsequently, these co-cultured organoids were dissociated, stained, sorted and quantified for the respective cell populations. Co-culture of IsoHD1 organoid with IsoHD1 iMac saw a significant reduction in the neuronal population when compared to control organoids that did not underwent co-culture. Conversely, coculture with mutant HD1 iMac saw a smaller degree of neurons reduction but was not significant (**Fig 6C**). Next, co-culture of IsoHD2 organoid with IsoHD2 iMac saw a slight reduction in neuronal population that was not statistically significant, while the co-culture with mutant HD2 iMac saw no difference when compared with control organoids (**Fig 6D**). Interestingly, we did not detect any change in the NPC population for either HD1 or HD2 after co-culture, likely because their numbers were relatively low to begin with due to the cellular composition of the forebrain organoid. Similarly, the iMac population was also small in all co-cultures. Transcriptomic analysis of the neurons of HD2 co-culture saw the mutant iMac co-culture having upregulated expression of genes associated with mitochondrial respiration (BCS1L, MRPL18, TSFM, MRPL11, MRPS30) but this phenomenon was not present in the isogenic iMac co-culture (**Fig 6E**). Conversely, transcriptomic analysis of the NPCs of HD2 co-culture saw the isogenic iMac co-culture having upregulated expression of genes associated with mitochondrial respiration (**Fig 6F**). Taken together, our model suggests that HDLS mutation affects neuronal population in a microglia-dependent manner and that this phenomenon is variable and mutation-dependent.

DISCUSSION

HDLS is an incurable neurodegenerative disease that begins in adulthood, progresses rapidly and has a grim prognosis. Efforts to elucidate the functional or dysfunctional aspects of the causative mutations in the *CSF-1R* gene have been hampered by the lack of an accurate disease model that recapitulates the human pathology: although rodent and zebrafish models have been generated and imparted valuable insights towards HDLS (13-16), discrepancies and limitations in each case have led to incomplete recapitulation of the disease's pathology, specifically in microglia numbers within brain regions and the effects on respective cognitive and sensorimotor tests. Additionally, a model looking into immune-neuronal crosstalk to better understand a neurodegenerative disorder that is primarily associated with microgliopathy, is important to advance the field. Here, we first generated iPSC lines from two patients with HDLS and then used CRISPR/Cas9 technology to reinstate a fully functional *CSF-1R* gene into some of the lines. While the generation of an HDLS donor-derived iPSC cell line has been reported (32), no other *in vitro* studies have yet reverted the causative mutation to wild type; a necessary step to understanding the direct impacts of diminished/absent CSF-1R signaling.

We then generated and characterized iMacs - precursors of microglia - from these lines, which exhibited typical morphology, phenotype and phagocytic capacity that were not obviously affected by *CSF-1R* mutation. Although we were able to generate phenotypically and functionally similar iMac across these lines for example for phagocytic capability, iMac yield varied greatly between the cell lines with a 50% lower yield for Mut

HD1 compared to IsoHD1 and, conversely, a higher yield for Mut HD2 200% compared to IsoHD2. This fundamental difference could be attributed to their respective mutations: the nonsense mutation identified in HD2 could not only more profoundly affect receptor signaling, but might also be a major factor during the course of gene editing leading to incomplete reversion to wild type at the epigenetic level, which we speculate was not the case for IsoHD1. Additionally, this observation could also be attributable to a reduced CSF-1 sensitivity in HD2 Mut iMacs as compared to HD1 Mut iMacs and we speculate that this would potentially give rise to the generation and subsequent maintenance of immature iMacs that lacks maturation even after terminally differentiated into tissue-resident macrophages.

Functionally, while phagocytosis of *E.Coli* beads was similar across lines, the baseline cytokine production as well as after phagocytosis of apoptotic neuronal cell line was different with an increase of IL-1β secretion in both mutant HD1 and HD2, compared to isogenic HD1 and HD2 iMacs. In the case of phagocytosis of apoptotic cells, this was not due to a difference in phagocytic activity as all cells were able to phagocytose apoptotic cells at a similar level. Importantly, higher levels of baseline pro- and anti-inflammatory cytokine production in the control group without apoptotic cells were observed within HD1 mutant, and both HD1 and HD2 mutant iMacs respectively. This suggest that mutant iMacs are innately in a more reactive or activated state when compared to isogenic iMacs and could reflect the reactive phenotype of HDLS-associated microglia and macrophage identified *in vivo* (10, 12). Conversely, isogenic iMacs seems to adopt less of the reactive phenotype with the reverted mutation as identified with an overall lesser cytokine production level. Importantly, such reactive phenotype was also highlighted by our

transcriptomic and metabolic profiling with upregulated pathways involving pro-inflammatory cytokines and preferential utilization of the glycolytic pathways in the mutant groups, a feature of macrophage activation (33, 34), respectively.

We subsequently incorporated donor-specific and their isogenic controls into a co-culture system using 3D forebrain organoids and iPSC-derived macrophages to better study HDLS. Isogenic and mutant iMacs co-cultured separately with their respective isogenic forebrain organoid differentiate into microglia-like cells with 23 days of coculture as shown by the expression of the microglial marker IBA-1, their ramified morphology as well as their transcriptomic profiles with up-regulation of genes associated with biological pathways that are typical of microglia functions such as neurodevelopment, neurodifferentiation, neurogenesis and brain development.

Subsequently, we analyzed the size of the organoids before and after co-culture as we recently showed that addition of iMac modulated NPC differentiation, limiting their proliferation and promoting axonogenesis, resulting in a reduction of co-culture organoid size (18). Here, while we noticed a significant decreased in the size of isogenic HD1 forebrains co-cultured with isogenic HD1 iMac compared to isogenic HD1 organoids, we did not measure any significant change in organoid size in the isogenic HD1 organoids co-cultured with mutant HD1 iMacs. This suggested that the crosstalk between iMicro and NPC is dysregulated in the context of the HD1 mutation. Since we showed that such size reduction is mediated by cholesterol transfer from iMicro to NPC, further work will be required to characterize cholesterol metabolism of HD iMac.

While we did not observe major changes in cell type composition in these cocultures, transcriptomic analysis of neuronal and NPC population after co-culture showed an increase in mitochondrial respiratory pathways associated genes in the mutant HD2 iMac co-culture neuron and isogenic HD2 iMac co-culture NPCs population respectively. This suggests increased metabolic rates in these respective populations that are contributed to by the different variants of iMac during co-culture, and show that mutated iMicro can change the states of non-mutated isogenic organoid cells. A parallel process *in vivo* would likely have profound long-term consequences for brain development and homeostasis.

Altogether, we propose that CSF-1R mutation in HDLS may cause subtle yet impactful disruptions to microglia homeostasis due to abnormal metabolic functions in the developing fetal brain, that subsequently compound and result in aberrant microglia functions during adulthood. This could also be mediated by upregulated pro-inflammatory cytokine production such as IL-1β at a basal level or upon clearing of cellular debris during development and adulthood homeostasis. IL-1β is of particular interest as numerous studies reported the role of IL-1β in neuroinflammation and neurodegeneration especially within the field of Alzheimer's disease: for example, postmortem brain sample analysis revealed elevated levels of Il-1β production, including around amyloid beta plaques; all suggestive of pathology-associated inflammation (35-37). Hence, we speculate that in CSF-1R$^{+/-}$ mutant microglia, which already have a predisposition towards increased secretion of IL-1β, are constantly being activated by IL-1β, either autocrine or paracrine, creating a dysfunctional neuro-environment that contributes to HDLS pathology. As such, experimental models looking to block or reduce IL-1β levels in the brain using the human mAb, canakinumab, targeting the proinflammatory cytokine IL-1β (38, 39), during both health and disease could be a potential target for therapy and may help to ameliorate HDLS pathology.

While no model perfectly recapitulates the full complexity of a disease, the application of iPSC-derived organoid co-culture approaches to primary patient-derived cells offers a valuable way to study the disease mechanisms of this rare pathology using human cells. Future studies employing microglia-sufficient patient-derived brain organoids have the potential to shed much-needed light into the pathogenesis of HDLS and other neurodegenerative diseases.

REFERENCES

1. Marotti JD, Tobias S, Fratkin JD, ea. Adult onset leukodystrophy with neuroaxonal spheroids and pigmented glia: report of a family, historical perspective, and review of the literature. Acta Neuropathol. 2004;107(6):481-8.
2. Papapetropoulos S, Pontius A, Finger E, Karrenbauer V, Lynch DS, Brennan M, et al. Adult-Onset Leukoencephalopathy With Axonal Spheroids and Pigmented Glia: Review of Clinical Manifestations as Foundations for Therapeutic Development. Front Neurol. 2021;12:788168.
3. Rademakers R, Baker M, Nicholson AM, Rutherford NJ, Finch N, Soto-Ortolaza A, et al. Mutations in the colony stimulating factor 1 receptor (CSF1R) gene cause hereditary diffuse leukoencephalopathy with spheroids. Nat Genet. 2011;44(2):200-5.
4. Zhuang LP, Liu CY, Li YX, Huang HP, Zou ZY. Clinical features and genetic characteristics of hereditary diffuse leukoencephalopathy with spheroids due to CSF1R mutation: a case report and literature review. Ann Transl Med. 2020;8(1):11.
5. Pridans C, Sauter KA, Baer K, Kissel H, Hume DA. CSF1R mutations in hereditary diffuse leukoencephalopathy with spheroids are loss of function. Sci Rep. 2013;3:3013.
6. Biundo F, Chitu V, Shlager GGL, Park ES, Gulinello ME, Saha K, et al. Microglial reduction of colony stimulating factor-1 receptor expression is sufficient to confer adult onset leukodystrophy. Glia. 2021;69(3):779-91.
7. Tay TL, Savage JC, Hui CW, Bisht K, Tremblay ME. Microglia across the lifespan: from origin to function in brain development, plasticity and cognition. J Physiol. 2017;595(6):1929-45.
8. Hammond TR, Robinton D, Stevens B. Microglia and the Brain: Complementary Partners in Development and Disease. Annu Rev Cell Dev Biol. 2018;34:523-44.
9. Bachiller S, Jimenez-Ferrer I, Paulus A, Yang Y, Swanberg M, Deierborg T, et al. Microglia in Neurological Diseases: A Road Map to Brain-Disease Dependent-Inflammatory Response. Front Cell Neurosci. 2018;12:488.
10. Kempthorne L, Yoon H, Madore C, Smith S, Wszolek ZK, Rademakers R, et al. Loss of homeostatic microglial phenotype in CSF1R-related Leukoencephalopathy. Acta Neuropathol Commun. 2020;8(1):72.
11. Konno T, Kasanuki K, Ikeuchi T, Dickson DW, Wszolek ZK. CSF1R-related leukoencephalopathy: A major player in primary microgliopathies. Neurology. 2018;91(24):1092-104.
12. Tada M, Konno T, Tada M, Tezuka T, Miura T, Mezaki N, et al. Characteristic microglial features in

patients with hereditary diffuse leukoencephalopathy with spheroids. Ann Neurol. 2016;80(4):554-65.
13. Chitu V, Gokhan S, Gulinello M, Branch CA, Patil M, Basu R, et al. Phenotypic characterization of a Csf1r haploinsufficient mouse model of adult-onset leukodystrophy with axonal spheroids and pigmented glia (ALSP). Neurobiol Dis. 2015;74:219-28.
14. Patkar OL, Caruso M, Teakle N, Keshvari S, Bush SJ, Pridans C, et al. Analysis of homozygous and heterozygous Csf1r knockout in the rat as a model for understanding microglial function in brain development and the impacts of human CSF1R mutations. Neurobiol Dis. 2021;151:105268.
15. Stables J, Green EK, Sehgal A, Patkar OL, Keshvari S, Taylor I, et al. A kinase-dead Csf1r mutation associated with adult-onset leukoencephalopathy has a dominant inhibitory impact on CSF1R signalling. Development. 2022;149(8).
16. Berdowski WM, van der Linde HC, Breur M, Oosterhof N, Beerepoot S, Sanderson L, et al. Dominant-acting CSF1R variants cause microglial depletion and altered astrocytic phenotype in zebrafish and adult-onset leukodystrophy. Acta Neuropathol. 2022;144(2):211-39.
17. Wang X, Zhang JB, He KJ, Wang F, Liu CF. Advances of Zebrafish in Neurodegenerative Disease: From Models to Drug Discovery. Front Pharmacol. 2021;12:713963.
18. Park DS, Kozaki T, Tiwari SK, Moreira M, Khalilnezhad A, Torta F, et al. iPS-cell-derived microglia promote brain organoid maturation via cholesterol transfer. Nature. 2023;623(7986):397-405.
19. Takata K, Kozaki T, Lee CZW, Thion MS, Otsuka M, Lim S, et al. Induced-Pluripotent-Stem-Cell-Derived Primitive Macrophages Provide a Platform for Modeling Tissue-Resident Macrophage Differentiation and Function. Immunity. 2017;47(1):183-98 e6.
20. Pinkus GS, Pinkus JL. Myeloperoxidase: a specific marker for myeloid cells in paraffin sections. Mod Pathol. 1991;4(6):733-41.
21. Elchaninov A, Lokhonina A, Vishnyakova P, Soboleva A, Poltavets A, Artemova D, et al. MARCO(+) Macrophage Dynamics in Regenerating Liver after 70% Liver Resection in Mice. Biomedicines. 2021;9(9).
22. Kolliniati O, Ieronymaki E, Vergadi E, Tsatsanis C. Metabolic Regulation of Macrophage Activation. J Innate Immun. 2022;14(1):51-68.
23. Jha AK, Huang SC, Sergushichev A, Lampropoulou V, Ivanova Y, Loginicheva E, et al. Network integration of parallel metabolic and transcriptional data reveals metabolic modules that regulate macrophage polarization. Immunity. 2015;42(3):419-30.
24. Xue J, Schmidt SV, Sander J, Draffehn A, Krebs W, Quester I, et al. Transcriptome-based network analysis reveals a spectrum model of human macrophage activation. Immunity. 2014;40(2):274-88.
25. Freeman SH, Hyman BT, Sims KB, Hedley-Whyte ET, Vossough A, Frosch MP, et al. Adult onset leukodystrophy with neuroaxonal spheroids: clinical, neuroimaging and neuropathologic observations. Brain Pathol. 2009;19(1):39-47.
26. Sundal C, Lash J, Aasly J, Oygarden S, Roeber S, Kretzschman H, et al. Hereditary diffuse leukoencephalopathy with axonal spheroids (HDLS): a misdiagnosed disease entity. J Neurol Sci. 2012;314(1-2):130-7.
27. Lancaster MA, Renner M, Martin CA, Wenzel D, Bicknell LS, Hurles ME, et al. Cerebral organoids model human brain development and microcephaly. Nature. 2013;501(7467):373-9.
28. Ormel PR, Vieira de Sa R, van Bodegraven EJ, Karst H, Harschnitz O, Sneeboer MAM, et al. Microglia innately develop within cerebral organoids. Nat Commun. 2018;9(1):4167.
29. Wake H, Moorhouse AJ, Nabekura J. Functions of microglia in the central nervous system--beyond the immune response. Neuron Glia Biol. 2011;7(1):47-53.
30. Cunningham CL, Martinez-Cerdeno V, Noctor SC. Microglia regulate the number of neural

precursor cells in the developing cerebral cortex. J Neurosci. 2013;33(10):4216-33.
31. Sierra A, Encinas JM, Deudero JJ, Chancey JH, Enikolopov G, Overstreet-Wadiche LS, et al. Microglia shape adult hippocampal neurogenesis through apoptosis-coupled phagocytosis. Cell Stem Cell. 2010;7(4):483-95.
32. Wu J, Tian W, Zhan F, Luan X, Cao L. Generation of an human induced pluripotent stem cell JTUi007-A from a patient with CSF1R-related leukoencephalopathy carrying heterozygous p.Ile794Thr mutation in CSF1R gene. Stem Cell Res. 2021;57:102593.
33. Liu Y, Xu R, Gu H, Zhang E, Qu J, Cao W, et al. Metabolic reprogramming in macrophage responses. Biomark Res. 2021;9(1):1.
34. Viola A, Munari F, Sanchez-Rodriguez R, Scolaro T, Castegna A. The Metabolic Signature of Macrophage Responses. Front Immunol. 2019;10:1462.
35. Cacabelos R, Alvarez XA, Fernandez-Novoa L, Franco A, Mangues R, Pellicer A, et al. Brain interleukin-1 beta in Alzheimer's disease and vascular dementia. Methods Find Exp Clin Pharmacol. 1994;16(2):141-51.
36. Shaftel SS, Griffin WS, O'Banion MK. The role of interleukin-1 in neuroinflammation and Alzheimer disease: an evolving perspective. J Neuroinflammation. 2008;5:7.
37. Italiani P, Puxeddu I, Napoletano S, Scala E, Melillo D, Manocchio S, et al. Circulating levels of IL-1 family cytokines and receptors in Alzheimer's disease: new markers of disease progression? J Neuroinflammation. 2018;15(1):342.
38. Ridker PM, Thuren T, Zalewski A, Libby P. Interleukin-1beta inhibition and the prevention of recurrent cardiovascular events: rationale and design of the Canakinumab Anti-inflammatory Thrombosis Outcomes Study (CANTOS). Am Heart J. 2011;162(4):597-605.
39. Yuan B, Clowers MJ, Velasco WV, Peng S, Peng Q, Shi Y, et al. Targeting IL-1beta as an immunopreventive and therapeutic modality for K-ras-mutant lung cancer. JCI Insight. 2022;7(11).

Supp Table 1: Demographics of HDLS patients

HD #	Sex	Age	Mutation
1	M	42	Exon 18; c.2381T>C (Ile794Thr)
2	F	32	Exon 15; c.2026C>T (p.Arg676Ter)

Supp Table 2: Primer list used for qPCR

Name	Forward Primer	Reverse Primer
Human IFN-g	TCGGTAACTGACTTGAATGTCCA	TCGCTTCCCTGTTTTAGCTGC
Human TNF-α	CCTCTCTCTAATCAGCCCTCTG	GAGGACCTGGGAGTAGATGAG
Human IL-1β	ATGATGGCTTATTACAGTGGCAA	GTCGGAGATTCGTAGCTGGA
Human IL-18	TCTTCATTGACCAAGGAAATCGG	TCCGGGGTGCATTATCTCTAC
Human IL-10	GACTTTAAGGGTTACCTGGGTTG	TCACATGCGCCTTGATGTCTG
Human TGF-β	GGCCAGATCCTGTCCAAGC	GTGGGTTTCCACCATTAGCAC
Human IL-6	ACTCACCTCTTCAGAACGAATTG	CCATCTTTGGAAGGTTCAGGTTG
Human IL-12b	ACCCTGACCATCCAAGTCAAA	TTGGCCTCGCATCTTAGAAAG
HPRT1	TGACCAGTCAACAGGGGAC	TGCCTGACCAAGGAAAGC
Mouse IFN-g	GCCACGGCACAGTCATTGA	TGCTGATGGCCTGATTGTCTT
Mouse TNF-α	CAGGCGGTGCCTATGTCTC	CGATCACCCCGAAGTTCAGTAG
Mouse IL-1β	GAAATGCCACCTTTTGACAGTG	TGGATGCTCTCATCAGGACAG
Mouse IL-18	GTGAACCCCAGACCAGACTG	CCTGGAACACGTTTCTGAAAGA
Mouse IL-10	CTTACTGACTGGCATGAGGATCA	GCAGCTCTAGGAGCATGTGG
Mouse TGF-β	CCACCTGCAAGACCATCGAC	CTGGCGAGCCTTAGTTTGGAC
Mouse IL-6	CTGCAAGAGACTTCCATCCAG	AGTGGTATAGACAGGTCTGTTGG
Mouse IL-12b	GTCCTCAGAAGCTAACCATCTCC	CCAGAGCCTATGACTCCATGTC
GAPDH	AGGTCGGTGTGAACGGATTTG	GGGGTCGTTGATGGCAACA

Supp Table 3: List of Reagents

Reagent	Source	Identifier
Dulbecco's Modified Eagle Medium (DMEM)	Corning	Cat # 10-014-CV
Fetal Bovine Serum	Gibco	Cat # 26140079
Penicillin/Streptomycin	Gibco	Cat # 15140122
Antibiotic-Antimycotic	Gibco	Cat # 15240062
Phosphate buffered saline	Corning	Cat # 21-040-CV
TeSR-E7	Stemcell	Cat # 5914
Epi5 Episomal reprogramming kit	Invitrogen	Cat # A15960
mTeSR-1	Stemcell	Cat # 85850
Matrigel	Corning	Cat # 354234
TrueCut Cas9 Protein V2	Thermofisher	Cat # A36498
CloneR	Stemcell	Cat # 05888
Rock inhibitor; Y-27632 (Dihydrochloride)	Stemcell	Cat # 72302
Human stem cell nucleofector starter kit	Lonza	Cat # VPH-5002
Human dermal fibroblast nucleofector kit	Lonza	Cat # VPD-1001
PSC 4-Marker Immunocytochemistry Kit	Thermofisher	Cat # A24881
StemPro-34 SFM	Gibco	Cat # 10639011
IMDM (Iscove's Modified Dulbecco's Medium)	Gibco	Cat # 1980030
Ham's F-12 Nutrient Mix	Gibco	Cat # 11765054
DMEM/F-12	Gibco	Cat # 11320033
L-glutamine	Gibco	Cat # 25030081
Ascorbic acid	Sigma	Cat # A4544
MTG (1-Thioglycerol)	Sigma	Cat # M6145
Human Transferrin	Roche	Cat # 10-652-202-001
CHIR99021	Sigma	Cat # SML1046-5MG
Recombinant Human BMP-4	Peprotech	Cat # 120-05
Recombinant Human VEGF	Peprotech	Cat # 100-20
Recombinant Human FGF-basic	Peprotech	Cat # 100-18B
Recombinant Human DKK-1	Peprotech	Cat # 120-30

Recombinant Human SCF (c-kit)	Peprotech	Cat # 300-07
Recombinant Human IL-3	R&D Systems	Cat # 203-IL
Recombinant Human IL-6	R&D Systems	Cat # 206-IL
Recombinant Human M-CSF	Peprotech	Cat # 300-25
N-2 Supplement (100X)	Gibco	Cat # 17502048
B27 Supplement (50X)	Gibco	Cat # 17504044
Bovine serum albumin	Yeasen	Cat # 36101ES76
KnockOut Serum Replacement	Gibco	Cat # 10828028
GlutaMAX Supplement	Gibco	Cat # 35050061
MEM Non-Essential Amino Acids Solution (100X)	Gibco	Cat # 11140050
2-Mercaptoethanol	Gibco	Cat # 21985023
Dorsomorphine	Sigma	Cat # P5499
A-83	Sigma	Cat # SML0788-5MG
SB-431542	Sigma	Cat # S4317-5MG
Human insulin	Absin	Cat # abs42225219
Triton X 100	MERCK	Cat # X100
RapiClear	SUNJin Lab	Cat # RC147001
SMART-Seq HT kit	Takara	Cat # 634437
TRIzol Reagent	Invitrogen	Cat # 15596018
VAHTS DNA Clean beads	Vazyme	Cat # N411-01-AA
Qubit dsDNA HS Assay Kit	Invitrogen	Cat # Q33231
TruePrep DNA library prep kit V2 for illumina	Vazyme	Cat # TD502-02
MTT test	Absin	Cat # abs50010-500T
Wright-Giemsa staining kit	BASO	Cat # BA-4017
pHrodo Red *E.coli* bioparticles conjugate	Invitrogen	Cat # P35361
PrimeScript RT Reagent Perfect Real Time kit	Takara	Cat # RR037B
ChamQ SYBR® Color qPCR Master Mix Low ROX Premixed	Vazyme	Cat # Q431-02
Paraformaldehyde	Yuanye Bio	Cat # r20497
TrypLE Express	Gibco	Cat # 12604013

ReLeSR	Stemcell	Cat # 100-0483
Accutase	Stemcell	Cat # 07920
GlycoBlue Coprecipitant	Thermofisher	Cat # AM9515
BD IMag™ Anti-CD11b Magnetic Particles - DM	BD Biosciences	Cat # 558013
Percoll	Cytiva	Cat # 17089101
IC Fixation Buffer	Invitrogen	Cat # 00-8222-49
Permeabilization Buffer 10X	Invitrogen	Cat # 00-8333-56
DAPI	ThermoFisher	Cat # D1306

Supp Table 4: Cell culture medium

Medium	Composition
Human dermal fibroblast medium	DMEM supplemented with 10% FBS, 1% Antimycotics/Antibiotics
StemPro-34 SFM Medium	Stempro-34 SFM, supplemented with 200 ug/mL Human Transferrin, 2 mM Glutamic Acid, 1x Pen/Strep (P/S), 0.5 mM Ascorbic Acid and 0.45 mM MTG.
Serum-Free Differentiation Medium (SF-Diff)	75% IMDM with Glutamax, 25% F12, 1x N2 supplement, 1x B27 Supplement, 0.05% BSA and 1x Pen/Strep.
Forebrain organoid first medium (F1M)	DMEM/F12 supplemented with 20% Knockout serum, 1x GlutaMax, 1x MEM-NEAA, 1x 2-Mercaptoethanol, 1x Pen/strep, Dorsomorphine 2 uM, A-83 2 uM
Forebrain organoid second medium (F2M)	DMEM/F12 supplemented with 1x N2 supplement, 1x GlutaMax, 1x MEM-NEAA, 1x Pen/Strep, CHIR-99021 1 uM, SB-431542 1 uM
Forebrain organoid third medium (F3M)	DMEM/F12 supplemented with 1x N2 supplement, 1x B27 supplement, 1x GlutaMax, 1x MEM-NEAA, 1x 2-Mercaptoethanol, 1x Pen/Strep, Insulin 2.5 ug/ml

Supp Table 5: Antibody list

Antibody	Source	Identifier
Rabbit anti-SOX2	Abcam	Cat # Ab97959
Goat anti IBA-1	Abcam	Cat # Ab5076
Mouse anti-NESTIN	Merck	Cat # MAB5326
Mouse anti-CD15 (SSEA-1)	Biolegend	Cat # 323033
Mouse anti-CD24	BDBioscience	Cat # 561646
Mouse anti-CD44	Biolegend	Cat # 338805
Mouse anti-CXCR4 (CD184)	Biolegend	Cat # 306515
Mouse anti-CD271	BDBioscience	Cat # 743358
Alexa-Fluor ® 488-conjugated Goat anti-mouse	Abcam	Cat # Ab150135
Alexa-Fluor ® 594-conjugated Goat anti-rabbit	Abcam	Cat # Ab150080
Alexa-Fluor ® 647-conjugated Donkey anti-goat	Abcam	Cat # Ab150135
CFSE		
Annexin V - PE	BD Pharmingen	Cat # 559763
Rabbit anti-OCT4	Invitrogen	Cat # A24867
Mouse anti-SSEA4	Invitrogen	Cat # A24866
Rat anti-SOX2	Invitrogen	Cat # A24759
Mouse anti-TRA-1-60	Invitrogen	Cat # A24868
Alexa Fluor™ 594 donkey anti-rabbit	Invitrogen	Cat # A24870
Alexa Fluor™ 488 goat anti-mouse IgG3	Invitrogen	Cat # A24877
Alexa Fluor™ 488 donkey anti-rat	Invitrogen	Cat # A24876
Alexa Fluor™ 594 goat anti-mouse IgM	Invitrogen	Cat # A24872
Anti-mouse CD115 BV605 (AFS98)	Biolegend	Cat # 135517
Anti-mouse Ly6G BV711 (1A8)	Biolegend	Cat # 127643
Anti-mouse Siglec F Alexa Fluor 647 (E50-2440)	BD	Cat # 562680
Anti-mouse CD11b BV650	Biolegend	Cat # 139309
Anti-mouse CD172a PerCP-eFluor® 710 (P84)	Biolegend	Cat # 46-1721-82
Anti-mouse Ly6C BV785 (HK1.4)	Biolegend	Cat # 128041
Anti-mouse CD45 BUV395 (30-F11)	BD	Cat # 565967

Figure and supplementary figure legends

Figure 1: Generation and characterization of iPSC lines from patients with HDLS

A) Schematic representation of the generation of patient-derived induced pluripotent stem cells (iPSC) from dermal fibroblasts, and the subsequent generation of isogenic controls via gene editing with CRISPR/Cas9. B) Sequencing of the genomic CSF-1R locus in donor-derived iPSC displaying mutant allele or genetically edited allele in isogenic control cell lines. C) Phase-contrast microscopy of mature reprogrammed iPSC colonies displaying typical hESC morphology. Images were acquired with a standard microscope (Nikon) with a 10 × objective. Scale bar represents 250 µM. D) Immunofluorescence imaging of Mut HD1 iPSC colonies for the pluripotency markers SOX2, OCT4, TRA-1-60 and SSEA-4. Scale bar represents 150 µM and 100 µM for left and right panel respectively. E) Cytogenetic analysis of IsoHD1 (left) and IsoHD2 (right) iPSC clone showing a normal karyotype.

Supp. Figure 1

A) Human dermal fibroblast outgrowth from skin biopsies after three weeks of culture. Images were acquired with a standard microscope (Nikon) with 10 x (left panel) and 20 x (right panel) objective respectively. Scale bar represents 200 µM. B) Phase-contrast microscopy (20 x) of emerging immature iPSC clones after reprogramming. Scale bar represents 200 µM. C) Sequencing of genomic CSF-1R locus displaying off-target events (OTE) analysis for IsoHD1 and IsoHD2 iPSC cell lines.

Figure 2: Generation and characterization of patient iPSC-derived macrophages

A) Schematic representation of the derivation of primitive macrophages from donor-derived iPSC. B) iMacrophage (iMac) yields across all cell line variants. C) Flow cytometry analysis of iPSC and iMac expression of macrophage surface markers CD45 and CD14. D) Morphology of iMacs visualized by Giemsa staining (left panel), and confocal imaging (middle panel); and internalization of PE-conjugated beads visualized by confocal imaging. Scale bar represents 30 µM. E) Uptake of pHrodo-labeled beads by iMacs in the presence and absence of cytochalasin D (Cyto D). F) Cell viability of iMacs used to determine CSF-1 sensitivity via an MTT assay, after incubating with varying concentrations of CSF-1 for seven days. Data are presented as mean ±SEM.

Figure 3: Mutant and isogenic control iMacs have distinct gene expression profiles

A and D) PCA analysis, B and E) volcano plots and C and F) GO analysis, of mutant and

isogenic iMacs derived from HD1 and HD2 differentially expressed genes (DEGs) respectively. Representative curve of ECAR (G, O) and their respective quantified data (H-J, P-R) are shown. Representative curve of OCR (K, S) and their respective quantified data (L-N, T-V) are shown. Real-time assessment of bioenergetic profile between mutant and isogenic HD1 iMacs, measured using extracellular flux assay and a mitochondrial stress test. The following glycolytic parameters were calculated based on ECAR: B) glycolysis, C) glycolytic capacity, D) glycolytic reserve. Data shown as means + SEM, n=9. The following parameters were calculated based on OCR: F) basal, G) ATP production and H) maximal respiration. 2-DG = 2-deoxy-glucose, FCCP = carbonyl cyanide 4-trifluoromethoxy-phenylhydrazone. (n=3) Data are presented as mean ± SEM.

Figure 4: Cytokine profiling of iMacs saw upregulated levels of IL-1β when probed with apoptotic neuronal cells

(A-B) Levels of transcription of pro- and anti-inflammatory cytokine genes (IFNg, TNFa, IL-1b, IL-6, IL-18, IL-10, IL-12 and TGFb) quantified by qPCR. (+uv depicts UV-treated, -uv depicts non-UV treated). n=3 per cell line. Data are presented as mean ±SEM.

Supp. Figure 2

A) CFSE-labeled SH-SY5Y cells were either UV-treated (red) or untreated (blue) then after 24 hours were incubated with Annexin V/PE to determine the induction of apoptosis. Annexin V labeling was measured by flow cytometry (top panel) and visualized by fluorescence microscopy (bottom panel). B) Percentage of $CD45^{+}$ cells in iMac cultures from HD1 (top row) and HD2 (bottom row) that took up apoptotic SH-SY5Y cells, with cytochalasin D used as a negative control. Data are presented as mean ±SEM. Scale bar represents 30 μM.

Figure 5: iMacs differentiate into microglia-like cells in coculture with forebrain organoids

A) Schematic diagram of co-culture between Day 31 iMacs and forebrain organoid. B) Forebrain organoids depicted before, during and after co-culture with iMacs. Day 31 isogenic forebrain organoids derived from the respective donor iPSC cell line were cocultured with the same isogenic- and mutant-cell-line- derived Day 31 iMacs. 30,000 iMacs were cocultured with each respective organoid derived from HD1 and HD2. Figure shows matured organoids before and after the addition of iMacs during coculture. C) Three-dimensional visualization of co-cultured brain organoids after 23 days. Neurons were labeled for NESTIN and NPCs for SOX2. Microglia-like cells (IBA-1+) were

visualized on the surface of organoids. D) Flow cytometry analysis of neurons, NPCs, and macrophage populations within forebrain organoids after 23 days of coculture. E-F) Donor-derived iMacs in forebrain co-cultures undergo distinct changes in gene expression as observed in PCA analysis (E and H), volcano plots (F and I) and GO analysis (G and J) in both HD1 and HD2 variants. Scale bar represents 200 µM.

Supp. Figure 3

A) Progression of forebrain organoid development across 31 days. Cells were initially seeded singly before the formation of embryoid bodies (EB) was observed after 2-3 days. Healthy EBs grew and matured, as seen by the formation of distinct neural epithelium in the organoids between Days 12 and 31. Images were acquired with a standard microscope (Nikon) with a 10 × objective. Scale bar represents 200 µM. B) Immunofluorescence imaging of neuroepithelial rosette (red, SOX2+) in Day 13 organoid. Developmental cues further supported the formation and expansion of the organoid to develop neuroepithelial tubes or rosettes, which contain predominantly neural stem cells (NPCs) that mimic the developing embryonic human cerebral cortex. C) Immunocytochemical analysis of microglia-like cells (Iba1) after 23 days of co-culture with organoids. Scale bars represent 50 µM for low magnification and 10 µM for high magnification. D) Three-dimensional visualization of non-co-cultured brain organoids (Day 23). Neurons were labeled for NESTIN (green, cytoplasm) while the NPCs were labeled for SOX2 (red, cytoplasm). Microglia-like cells (IBA1+, white) were not identified, indicating the lack of formation of innately developing microglia. Scale bar represents 200 µM.

Figure 6: Co-culture results in impaired regulation of neurons within organoids

Size of A) HD1 and B) HD2 organoids measured before and after co-culture with mutant and isogenic iMacs in both HD1 and HD2 variants. The effects of co-culture on neuronal populations in C) HD1 and D) HD2 organoids after 23 days. Transcriptomic analysis of co-cultured E) neurons and F) NPCs from HD2 organoids after 23 days. Data are presented as mean ±SEM.

MATERIALS AND METHODS

Preparation of human dermal fibroblasts from donor biopsies

Samples from patients with HDLS were collected via skin punch and placed in biopsy medium [Gibco DMEM Glutamax supplemented with 1% 100x Antibiotics/Antimycotics (Gibco AB/AM) and 10% Fetal Bovine Serum (Gibco, FBS)] for transport to the laboratory. Immediately on arrival, biopsies were placed in 75% ethanol for 30 sec then washed three times with DMEM Glutamax supplemented with 1% AB/AM; attached adipose tissue was removed using sterile scissors before biopsies were cut into small $1mm^2$ cubes and placed dermis-side down onto a 6-well plate then left to dry slightly for 20 min to facilitate adhesion. Biopsy culture medium was then added and plates incubated overnight at 37°C, 5% carbon dioxide in air; 48 hrs later, the medium was changed then biopsies cultured for a further 10-14 days during which fibroblast outgrowth was observed. At around 90% confluency, fibroblasts were detached from the plates using 0.05% Trypsin/EDTA and passaged. Biopsies were re-plated up to three times for further fibroblast propagation.

Reprogramming of human dermal fibroblasts into induced pluripotent stem cells

Individual donor's fibroblasts were reprogrammed into induced pluripotent stem cells (iPSC) using the Epi5 Episomal reprogramming kit (Invitrogen), and the Human dermal

fibroblast nucleofector kit (Lonza) on a Lonza Nucleofector 2B device. Briefly, fibroblast cultures at approximately 90% confluency were detached from their plates using 0.025% Trypsin/EDTA then collected by centrifugation at 350 g for 5 min at room temperature. Cell pellets were resuspended in 100 µl of nucleofector solution at room temperature then counted: 200,000 cells were used per transfection with 1 µl of each of the episomal vectors, using program U-023. Transfected cells were subsequently plated onto Matrigel-coated (Stemcell) 6-well plates with 2 ml of pre-warmed fibroblast medium (DMEM supplemented with 10% FBS & 1% AB/AM) and incubated for two days. The medium was then replaced with 2 ml of TeSR-E7 medium, which was changed every two days for 25-35 days until early iPSC clones emerged.

Isolating iPSC colonies

Between days 25 and 35, colonies resembling human embryonic stem cell colonies emerged, were collected using a sterile needle under a stereomicroscope, mechanically fragmented, and added to 24-well plates pre-coated with Matrigel and containing 500 µl of mTeSR-1. The colonies were cultured for 24 hr then underwent medium change with fresh mTeSR-1 for 7-10 days until 80% confluent.

Culture and maintenance of iPSC cell lines

To passage, 500 ul of ReleSR were added into each well and incubated in 37°C for 3 min before tapping the plate firmly on all sides to dislodge the iPSC colonies. Subsequently, the iPSC fragments were transferred into 12-well plates and again cultured until approximately 80% confluent, before passaging into 6-well plates, all while maintaining in mTeSR-1 with daily medium change. Mature iPSC colonies were identified by their characteristic phenotype: clear distinct borders, high nuclei-to-cytoplasm ratio, and raised,

refractive, three-dimensional-like colonies.

Characterization of induced pluripotent stem cell colonies

Characterization of iPSC colonies was achieved using the PSC 4-Marker Immunocytochemistry Kit (Gibco). Briefly, spent mTeSR-1 medium was aspirated from the cells before adding 200 µl of fixative solution per well and incubating for 15 min at room temperature, which was then replaced by 200 µl of permeabilization solution for 15 min, then by 200 µl of blocking solution for 30 min. Subsequently, 2 µl of antibodies recognizing SSEA4 and OCT4 were added directly to the blocking solution and incubated for three hrs before washing three times with wash buffer (1x DPBS). Secondary antibodies were added at 0.8 µl per well and incubated for one hr at room temperature before washing three more times. During the last wash, one drop of NucBlue Fixed Cell Stain (DAPI) was added into the wash buffer and incubated for 5 min. Cells were either imaged immediately or stored at 4°C in the dark, for up to one month before analysis.

Karyotyping iPSC colonies

Mature iPSC colonies were pre-treated with 0.1 µg/ml of colcemid for 3 hr in the incubator before dissociation into single cells for imaging. Subsequently, cells were fixed with 4% PFA and sent for karyotype analysis at Zhen He Biotech, Shanghai.

Microscopy

Cell morphology observations were regularly performed using an Olympus CKX41 inverted microscope. Bright field and phase contrast images were taken using a Nikon Eclipse TS2 inverted microscope equipped with a Digital Sight camera. Images were processed using the proprietary software ImageView.

Differentiation of iPSC into primitive-like macrophages (iMacs)

Patient-derived iMacs were generated as previously described (1). Briefly, iPSCs were cultured in Stempro34 medium, supplemented with L-glutamine (100x) , ascorbic acid (5mg/ml), 1-Thioglycerol (26ul/2ml), Transferrin (200x) and Pen/Strep (1%), with the addition of CHIR99021 (2 µM), VEGF (50 ng/mL) and BMP4 (5 ng/mL) from days 0-2 to induce mesodermal lineage commitment; hemangioblast-like cell formation was then induced by culture in the presence of BMP4 (5 ng/mL), VEGF (50 ng/mL) and bFGF (20 ng/mL) on day 2 and only VEGF (15 ng/mL) and bFGF (5 ng/mL) on day four. From day 6-10, hemangioblasts were further committed to the generation of hematopoietic cells by the addition of DKK-1 (30 ng/mL), VEGF (10 ng/mL), bFGF (10 ng/mL), IL-6 (10 ng/mL), IL-3 (20 ng/mL) and SCF (50 ng/mL). To further promote the maturation of hematopoietic cells and CSF-1R expression, on days 12 and 14, medium was supplemented with SCF (50 ng/ml), bFGF (10 ng/ml), IL-6 (10 ng/ml) and IL-3 (20 ng/ml). From day 16 to day 31, the medium was switched to SF-Diff consisting of IMDM (75%) and F12 (25%) with the addition of N2 (100x), B27 (50x), 0.05% BSA, 1% Pen/Strep, supplemented with 50 ng/ml of CSF-1 to terminally differentiate the primitive cells to iMacs. Full medium changes were carried out every two days from days 0-14 and every three days from days 16-31. Free-floating cells were observed from as early as day six of culture and were collected and re-seeded back into individual wells during medium changes. Additionally, iMacs were initially cultured in a hypoxia incubator (5% O_2, 5% CO_2) from day 0–8 before moving into a normoxic incubator until day 31, when the cells were used for experiments. iMac identity was confirmed by flow cytometry with labeling for the macrophage markers CD45 and CD14.

Generation of forebrain organoids

Forebrain organoid generation was adapted from Qian *et al.*, (2), which described a guided differentiation method that requires various cytokines and growth factors to be added at different differentiation stages, as follows.

Stage 1 (days 0-4: embryoid body formation)

iPSC on 6-well plate at approximately 80% confluency were dissociated into single cells using Accutase (Stemcell) before counting and seeding at 50,000 cells per well into an ultra-low attachment (ULA) 96-well plate with 150 µl of forebrain first medium (F1M: DMEM/F12, 20% KOSR, 1x GlutaMax, 1x MEM-NEAA, 1x 2-Mercaptoethanol, Pen/strep, Dorsomorphine 2 µM, A-83 2 µM) and 20 µM of ROCK Inhibitor (Stemcell). Plates were incubated at 37°C and 5% CO_2 for 24 hrs (day -1). On day zero, medium was refreshed with the addition of 2 uM Dorsomorphin (Sigma) and 2 uM A83-01 (Sigma). Half medium changes were then performed on days two and four with the exclusion of ROCK inhibitor: small embryoid bodies (EB) were observed at this point.

Stage 2 (days 5–13: neuro-ectodermal induction)

On day five, one EB was transferred into each well of a ULA 24-well plate with 500 µl of Forebrain second medium (F2M: DMEM/F12, 1x N2 supplement, 1x GlutaMax, 1x MEM-NEAA, Pen/Strep, CHIR-99021 1 µM, SB-431542 1 µM). On day seven, healthy EB displaying a smooth and round surface were embedded individually into 20 µl of Matrigel, according to the method of Lancaster *et al.*, (3). Once the Matrigel had fully polymerized, eight embedded EBs were transferred into a 10 cm petri dish with 10 ml of F2M before incubating at 37°C with half medium changes every two days until day 13. At this point, cluster(s) of neuroepithelium buds were present in individual organoids, evident as neural tube-like structure without extending cell processes.

Stage 3 (days 14–31: maturation)

On day 14, Matrigel-embedded organoids were collected and replated, with the attached Matrigel removed by repeated pipetting, before being transferred into a clean 10 cm petri dish with eight ml of Forebrain third medium (F3M: DMEM/F12, 1x N2 supplement, 1x B27 supplement, 1x GlutaMax, 1x MEM-NEAA, 1x 2-Mercaptoethanol, Pen/Strep, Insulin 2.5 ug/ml). Dishes were incubated at 37°C on an orbital shaker at 80 rpm, with half F3M changes every three days until organoids were used for analysis/experiments.

Generation of isogenic clones using CRISPR/CAS9

sgRNAs were designed using the CRISPR design tool www.crispor.tefor.net and selected based on highest efficiencies as well as off-target scores and synthesized by GENESCRIPT with scaffold. ssDNA template was designed with 40bp of homologous nucleotides flanking both arms of the point of mutation, inclusive of silent mutations on, and adjacent to, the PAM region, and synthesized by Sangor Shanghai. Genome editing via homology-directed repair from the CRISPR/Cas9 system in combination with a ssDNA was used to guide the single nucleotide correction of the HDLS point mutation, according to donor's Sanger sequencing reports on Exon 15 (Donor #2) and 18 (Donor #1) of CSF-1R by homologous recombination.

The ribonucleoprotein (RNP) complex consisting of Cas9 protein and sgRNA was assembled using the Trucut V2 (Invitrogen) and Amaxa Human Stell Cell Nucleofector Starter Kit (VPH-5002). The RNP complex was subsequently transfected into dissociated iPSCs by electroporation with Lonza Nucleofector 2B using the Amaxa Human Stem Cell Nucleofector Starter Kit (Lonza) according to manufacturer's manual. After

electroporation, the cells were immediately plated onto Matrigel-coated 6-well plates containing mTeSR1 medium supplemented with 10 µM ROCK inhibitor (Stemcell) and CloneR (Stemcell) at various seeding densities to facilitate the harvesting of-clones. After 48 hrs, medium was refreshed with the removal of ROCK inhibitor; subsequently, medium was refreshed daily with the removal of both ROCK inhibitor and CloneR until clones were mature enough for manual picking. Individual clones were manually harvested and plated onto Matrigel-coated 24-well plates with mTesr-1 medium and 10 µM of ROCK inhibitor.

GuideRNA and ssDNA template used for targeting HDLS#1:

1) gRNA = TGGTCATGTGGCCAAGACTG
2) ssDNA=
GCGCGTAACGTGCTGTTGACCAATGGTCATGTAGCTAAAATCGGGGACT
TCGGGCTGGCTAGGGACATCATGAATGACTC
(Green nucleotide denotes a silent mutation)

GuideRNA and ssDNA template used for targeting HDLS#2:

1) gRNA = GCTCAACTTTCTGTGAAGGA
2) ssDNA=
CACGGAGTACTGTTGCTATGGCGACCTGCTCAATTTCCTTCGAAGAAAA
GCTGAAGCCATGCTGGGACCCAGCCTGAGCC
(Green nucleotide denotes a silent mutation)

Clones were screened for SNP editing using the ICE SYNTHEGO tool (https://ice.synthego.com) and off-target events (OTE) screened for using CRISP-ID software (http://crispid.gbiomed.kuleuven.be).

Co-culture of forebrain organoids and iMacs to generate iMicroglia

Co-culturing iMacs (primitive macrophages) with organoids enables the iMacs to be in a neurogenic niche environment where they would subsequently differentiate into iPSC-derived microglia (iMicro). Thirty thousand day 31 iMacs (mutant or Isogenic controls) were resuspended in F3M before adding onto their isogenic organoid in each well of an ULA 96-well plate. Cocultures were incubated for seven days with daily half F3M change supplemented with CSF-1 (100 ng/ml). On day eight, each organoid was transferred to an individual well of a ULA 24-well plate and supplemented with 1 ml of F3M and CSF-1 (100 ng/ml); half F3M change was performed every three days until analysis.

Clearing of forebrain organoids for 3D-imaging

Organoids were first fixed in 4% paraformaldehyde for 30 min at room temperature followed by washing twice in PBS then incubating in PBS overnight at 4°C. The next day, PBS was replaced with a permeabilization buffer (2% Triton X-100 in PBS solution) and organoids were incubated on an orbital shaker at room temperature for 72 hrs. At the end of permeabilization, organoids were incubated in blocking buffer (5% normal donkey serum, 5% normal goat serum, 1% Fetal Bovine Serum, 1% Triton X-100 in PBS solution) at 4°C overnight. Organoids were then incubated with primary antibodies at 1:200 in antibody dilution buffer (1% bovine serum albumin, 0.2% Triton X-100 in PBS solution) at 4°C for 72 hrs. Primary antibodies specific for the following markers were used: NESTIN (MERCK), SOX2 (Abcam), and IBA-1 (Abcam). Organoids were washed in washing buffer (1x PBS solution) on an orbital shaker at room temperature for one hr before being kept in 1x PBS solution at 4°C overnight. The organoids were subsequently incubated with the following secondary antibodies at 1:200 in antibody dilution buffer, at 4°C for 48 hrs: goat anti-mouse Alexa Fluor 488 (Biolegend), goat anti-rabbit Alexa Fluor

594 (Abcam), and donkey anti-goat Alexa Fluor 647 (Abcam). The organoids were then washed with wash buffer for one hr on an orbital shaker at room temperature then kept in PBS at 4°C overnight before counterstaining with the nuclear marker DAPI on an orbital shaker at room temperature for two hrs. Organoids were then washed twice in washing buffer on an orbital shaker at room temperature for one hr, then again kept overnight at 4°C in 1x PBS. The following day, organoids were transferred individually to confocal-imaging-compatible glass-bottomed containers and 20 µl of RapiClear (SUNJin Lab) solution was added onto each organoid and left until they were cleared (usually 24 hrs depending on the size of the organoid). Whole organoids were imaged using a FV3000 confocal microscope with 20× objective lens (Olympus, Japan) and analyzed using iMaris software (BITPLANE).

Measurement of area of organoid

Area of organoids were measured using ImageJ software. Briefly, the “freehand selection” tool was used to trace the circumference of each individual organoid. The average of three measurements was used as the final readout.

Dissociation of forebrain organoids

Organoids were collected individually using 200 µl pipette with a cut pipette tip and incubated in 500 µl of Accutase at 37°C with gentle pipetting after 10 min, then allowed to fully dissociate for another 5-15 min at 37°C as needed. After again pipetting, cells were suspended in 1 ml of MACS buffer and collected by centrifugation at ~~1350 rpm~~ 350 g at RT for 5 min. Cells were then used in experiments.

Flow cytometry

Cells were prepared for labeling by first washing in FACS buffer, then resuspending cells in 70 µl of Fc-block (1:200) and incubating for 20 min at 4°C. Subsequently, the primary

antibody cocktails were added into the cells at a 1:200 dilution before being vortexed and incubated for 30 min at 4°C. For samples that required secondary antibody labeling, after incubation with primary antibodies the cells were washed with FACS buffer before secondary antibodies (1:500) were added and incubated for 25 min at 4°C. After a further wash in FACS buffer, DAPI was added then cells were analysed using the BD Symphony X-50.

Cell sorting of cocultured organoids

Cells were isolated into sorting solution (SMART-Seq HT kit. 10X lysis buffer, RNase inhibitor, 3' SMART-Seq CDS Primer II A, nuclease-free water) using the BD Aria III cell sorter. After sorting, cell-containing tubes were briefly spun down and immediately placed in liquid nitrogen for snap freezing. Lysates were stored at -80°C.

RNA extraction of samples

RNA extraction was performed using Trizol according to the manufacturer's instructions. Briefly, 500 µl of Trizol was added to each sample before the addition of 100 µl of chlorofoam to each sample and mixed thrice (15 sec per succession) before incubating at room temperature for 5 min. Samples were then centrifuged at 20,000g, 20 min, 4°C before the organic solvent was transferred into new eppendorf tubes. One µl of GlycoBlue co-precipitate (Invitrogen) was added to each sample and mixed well before the addition of 250 µl of isoproponol. Samples were mixed well before incubating at -80°C for at least one hr. Thawed samples were subsequently centrifuged at 12,000g, 4°C for 15 min before decanting supernatant, washing again with ice-cold 75% ethanol and centrifuging at 7500g, 4°C for 5 min. Samples were left to air dry for approximately 5 min after decanting of supernatant, before the RNA pellet was resuspended in 10 µl of DPEC water and stored at -80°C.

cDNA library construction for RNA-sequencing

RNA samples from the previous step were first converted to complementary DNA (cDNA) using the Takara HT kit according to the manufacturer's instruction. Briefly, 5 µl of purified total RNA was added to 1 µl of 10X reaction buffer consisting of 10X lysis buffer and RNase inhibitor; 1 µl of 3' SMART-seq primer II A was added and mixed well by vortexing before incubating the samples at 72°C for 3 min. Samples were then immediately placed on ice for 2 min. A one-step master mix consisting of 0.7 µl of nuclease-free water, 8 µl of one-step buffer, 1 µl of SMART-Seq HT oligonucletide, 0.5 µl RNase inhibitor, 0.3 µl SeqAmp DNA polymerase, and 2 µl of SMARTscribe reverse transcriptase was subsequently added to each sample and mixed well. The following program was used to run the PCR protocol:

42°C		90 min
95°C		1 min
18 cycles:	98°C	10 sec
	65°C	30 sec
	68°C	3 min
72°C		10 min
4°C		Forever

The resulting cDNA product was purified using the Vazyme VAHTS DNA Clean beads. Briefly, 20 µl of beads were added to each cDNA product, mixed well and incubated for 5 min at RT before placing samples on a magnectic stand for 2 min. The supernatant was discarded and cDNA was washed twice with cold 80% ethanol before being air-dried for 3 min. Purified cDNA was subsequently eluted from the magnetic beads with 15 µl of DPEC water. The concentration of cDNA was measured with the Qubit dsDNA HS Assay Kit (Invitrogen) using the Qubit 4 fluorometer.

cDNA library construction was performed using the Vazyme TruePrep DNA library prep kit V2 for illumina according to the manufacturer's instructions. Briefly, the purified cDNA obtained from the previous step was diluted to a final concentration of 1ng/µl with sterile water. Next, 7.5 µl of Mix A (2 µl 5x TTBL, 2.5 µl TTE Mix V5, 3 µl DPEC water) was added to 2.5 µl of diluted cDNA and run using the Nextera-1 program at 55°C for 10 min.

TSS was immediately added to each sample and left to incubate at RT for 5 min before 7.5 µl of Mix B (2 ul DPEC water, 5 µl 5x TAB, 0.5 µl TAE) was added to each sample. 2.5 µl of N5 and N7 primer was added and mixed well before running on the Nextera-2 program:

72°C		3 min
98°C		3 min
	98°C	15 sec
13 cycles:	60°C	30 sec
	72°C	3 min
72°C		5 min
4°C		Forever

Subsequently, samples were purified using the vazyme beads and cDNA was eluted with 20 µl of DPEC water before measuring the concentration.

For pooling of cDNA libraries, 40 ng of each sample was added to a final volume of 40 µl, adjusted with DPEC water, and incubated with 22.6 µl of Vazyme clean beads at RT for 5 min before magnectic separation. The entire volumn of supernatant was transferred to a fresh PCR tube to which was added 6.4 µl of Vazyme clean beads. The contents were mixed well and incubated at RT for 5 min before separation: subsequently, the supernatant

was discarded and bead-bound-cDNA was washed twice with 80% ethanol before being air dried for 3 min. Purified pooled cDNA samples were eluted with 20 µl of DPEC water and tested for concentration.

Bulk RNA Analysis

The clean paired-ends reads were aligned to the GRCh38.96 human genome reference using kallisto (version 0.46.1) with parameters "–bootstrap-samples=100". The transcript-level estimated counts belonging to the same gene were then aggregated into the matrix of gene-level counts (TPM) implemented in the R package tximport (version 1.14.2).

Pairwise comparison across RNA-seq data was performed to get differentially expressed genes between each two types of cells, using the linear model and the empirical Bayes method implemented in R limma package (version 3.42.2), with significance thresholds for p-value<0.05 and log2(fold change)≥0.5 (Figure 3) or 1.5 (Figure 5). The differentially expressed genes identified with top log2(fold change) were selected to perform the PCA analysis in R using prcomp function. Additionally, the clusterProfiler package (version 4.10.0) was employed for pathway enrichment analysis via the compareCluster function and “enrichGO” method, targeting “ALL” GO ontologies.

Metabolic function using Seahorse analysis

The bioenergetic profile of iMacs was assessed by determining the oxygen consumption rate (OCR) and the extracellular acidification rate (ECAR) using an XF-96 Flux Analyzer (Seahorse Bioscience). Sensor cartridges (Agilent Technologies) were hydrated in XF Calibrant (Agilent Technologies) at 37°C overnight, devoid of carbon dioxide, following

the manufacturer's instructions. Cells were resuspended in either OCR XF base medium supplemented with 10 mM glucose, 2 mM L-glutamine and 1mM sodium pyruvate, or ECR XF base medium supplemented with 2 mM L-glutamine, before being seeded at 40,000 cells/50 µl/well into XF96 culture plates. Cells were pelleted by centrifugation at 200g for 1 min then resuspended in either 125 µl of OCR or ECR medium per well and incubated at 37°C in a CO_2-free incubator for 45 min before loading into the Seahorse analyzer. Cells were sequentially treated with 25 µl injections of specific bioenergtic modulators that were added to the wells prior to loading, to test for different paramters of mitochondrial and glycolytic functions. ECR analysis was probed with 10 mM glucose to stimulate glycolysis, followed by the addition of 2µM oligomycin to block ATP synthase and 50 mM 2-deoxy-glucose (2DG) to shut down the function of glycolysis. Conversely, OCR analysis was probed with 2 µM oligomycin, 1 µM FCCP (carbonyl cyanide-4-(trifluoromethoxy) phenylhydrazone) to stimulate maximal mitochondrial oxygen consumption and 0.5 µM rotenone plus antimycin A to asses OXPHOX parameters from the OCR levels. Mitochondrial and glycolytic parameters were calculated as recommended by the instrument manufacturer (Agilent Technologies).

MTT Test

On the day before testing, 25,000 iMacs were seeded into each well of a 96-well flat-bottom plate. The next morning, 20 µl of MTT solvent (10% of total volume) was added to each well and incubated at 37°C for 3.5 hrs before being decanted. Next, 200 µl of MTT formazan solvent was added to each well before being placed onto a shaker for 15min in the dark, then incubated RT for an additional 30 min in the dark. Measurements were read by a spectrophotometer at OD570 and OD690.

Cytospin assay

iMacs were first trypsinized using TryPLE express before being counted using the Countess II. Approximately 50,000 cells were resuspended in 150 µl of PBS before being transferred to a cytocentrifuge cytofunnel paired with a glass slide, and centrifuged for 5 min at 800rpm 200 g, air dried for 30 min before sealing with mounting medium. Images were acquired with an Olympus BX53 light microscope equipped with a 100x oil immersion objective lens.

Giemsa staining

Adequately air-dried slides were placed in a staining tray and flooded with 1ml per slide of Solution A of the Wright-Giemsa staining kit (BASO) for 1 min. Subsequently, 500 µl of Solution B was added to each slide and agitated for 5 min. Slides were then rinsed in distilled water for 5 min before being air-dried for 30 min then sealed in synthesis resin. Images were acquired with the Olympus BX53 light microscope paired with a 100X oil immersion objective lens.

Neuronal cell line SH-5YSY apoptosis induction

SH-5YSY cells were kindly provided by the lab of Xu Tien le from the Shanghai Institute of Immunology. SH-SY5Y cell monolayers in sterile PBS were exposed to UV-radiation for 30 min before collection of cells into serum-free medium (DMEM + 1% P/S) and incubation at 37°C overnight to induce apoptosis. The following day, cells were centrifuged at 350 g, RT for 3 min before staining with Annexin V (BD Pharmingen PE Annexin V apoptosis detection kit) for 20 min at RT in the dark, before being analyzed by flow cytometry.

Phagocytic assay with conjugated *E. coli* beads

First, pHrodo Red *E. coli*-conjugated bioparticles (Invitrogen) were reconstituted to a working concentration of 1 mg/ml with sterile water before adding to iMacs in complete medium at 1:10 final concentration. After incubation at 37°C for 45 min, cells were washed twice with PBS before collection for flow cytometry analysis.

RNA extraction and real-time quantitative PCR (qPCR)

Total RNA was extracted from each group with TRIzol Reagent (Invitrogen). The cDNA was obtained by using the PrimeScript RT Reagent Perfect Real Time kit (Takara, Japan). Briefly, 500 ng of RNA for each sample was amplified as a template, in 10 µl of reaction mixture (2 µl 5X PrimeScript buffer, 0.5 µl PrimeScript RT Enzyme Mix I, 0.5 µl Oligo dT Primer, 0.5 µl random 6-mers, RNA product, RNase-free water). This mixture was then incubated at 37°C for 15 min and subsequently at 85°C for 5 sec to obtain cDNA. qPCR was performed in a ViiA 7 Real-time PCR system (Applied Biosystems) with ChamQ SYBR® Color qPCR Master Mix Low ROX Premixed (Vazyme).

Statistical anslysis

Statistical tests were performed using GraphPad Prism 8.0.1 (GraphPad Software, La Jolla, CA, USA; www.graphpad.com). All experiments were performed in triplicate and data analysis was performed using unpaired Student's t-tests. All data represent the mean ± standard error of mean (SEM). Statistical significance was assigned as: $p < 0.05$ was considered significant: *$p < 0.05$; **$p < 0.01$; ***$p < 0.001$. $p > 0.05$ was considered nonsignificant (n.s.).

MATERIALS AND METHODS REFERENCES

1. Takata K, Kozaki T, Lee CZW, Thion MS, Otsuka M, Lim S, et al. Induced-Pluripotent-Stem-Cell-Derived Primitive Macrophages Provide a Platform for Modeling Tissue-Resident Macrophage Differentiation and Function. Immunity. 2017;47(1):183-98 e6.

2. Qian X, Jacob F, Song MM, Nguyen HN, Song H, Ming GL. Generation of human brain region-specific organoids using a miniaturized spinning bioreactor. Nat Protoc. 2018;13(3):565-80.

3. Lancaster MA, Renner M, Martin CA, Wenzel D, Bicknell LS, Hurles ME, et al. Cerebral organoids model human brain development and microcephaly. Nature. 2013;501(7467):373-9.

Figure 1

A

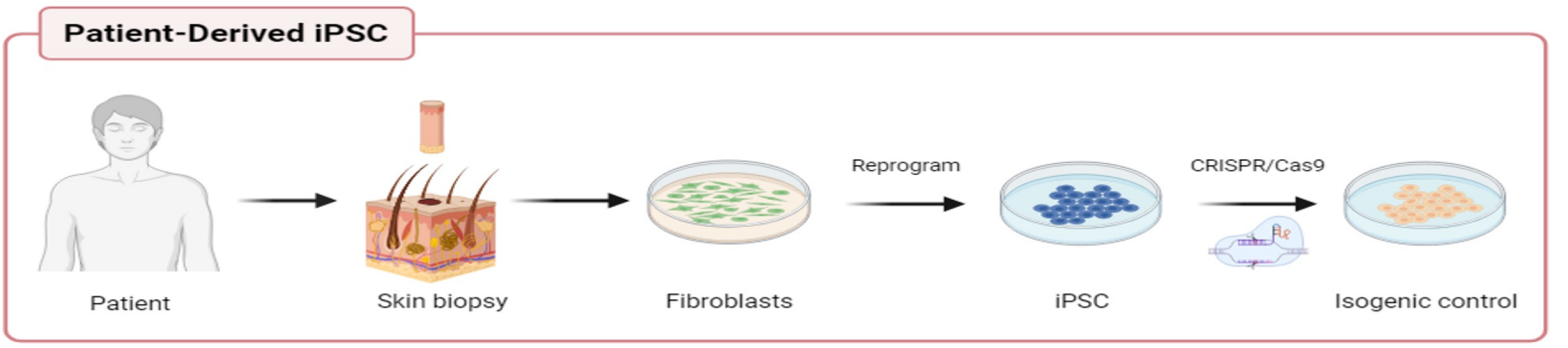

B

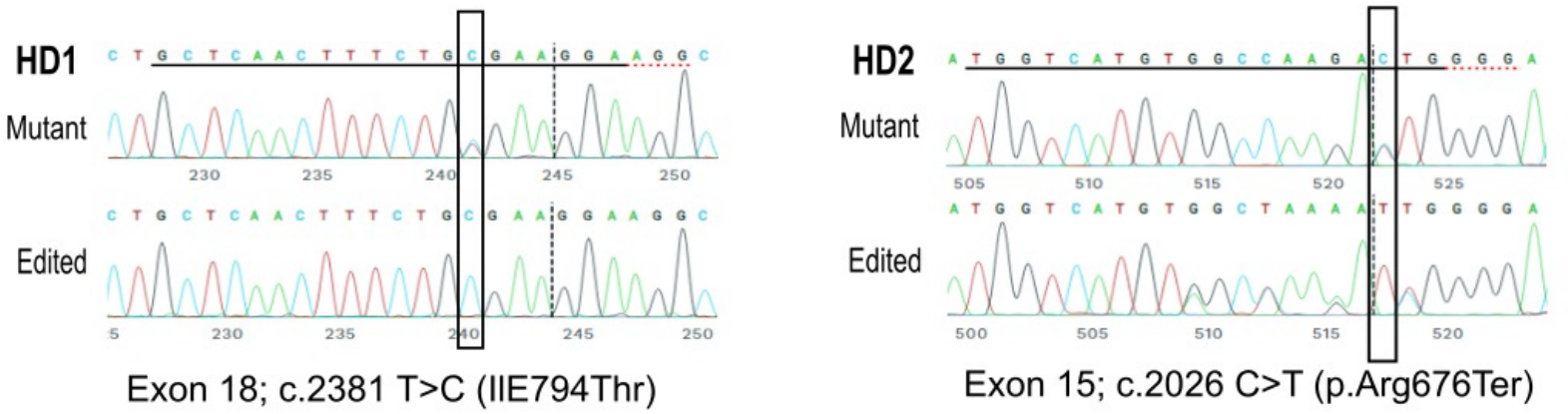

C

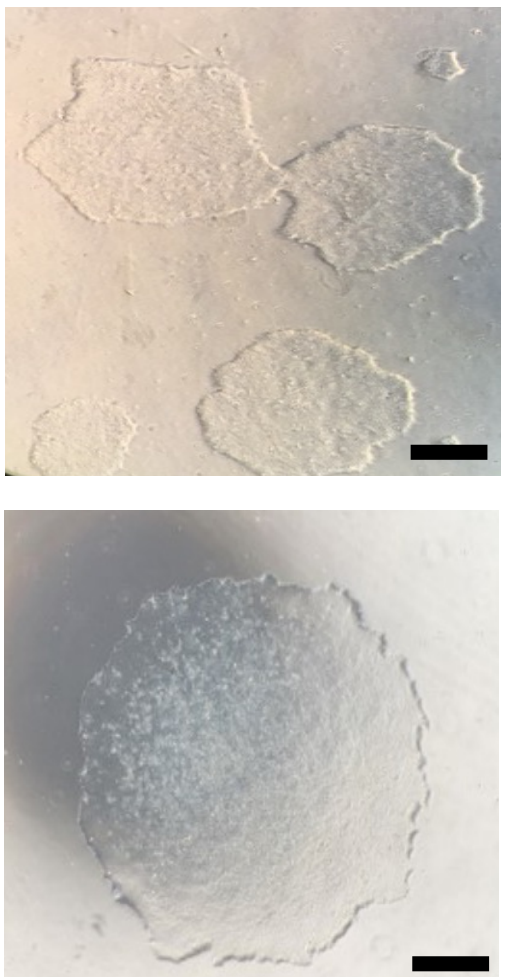

D

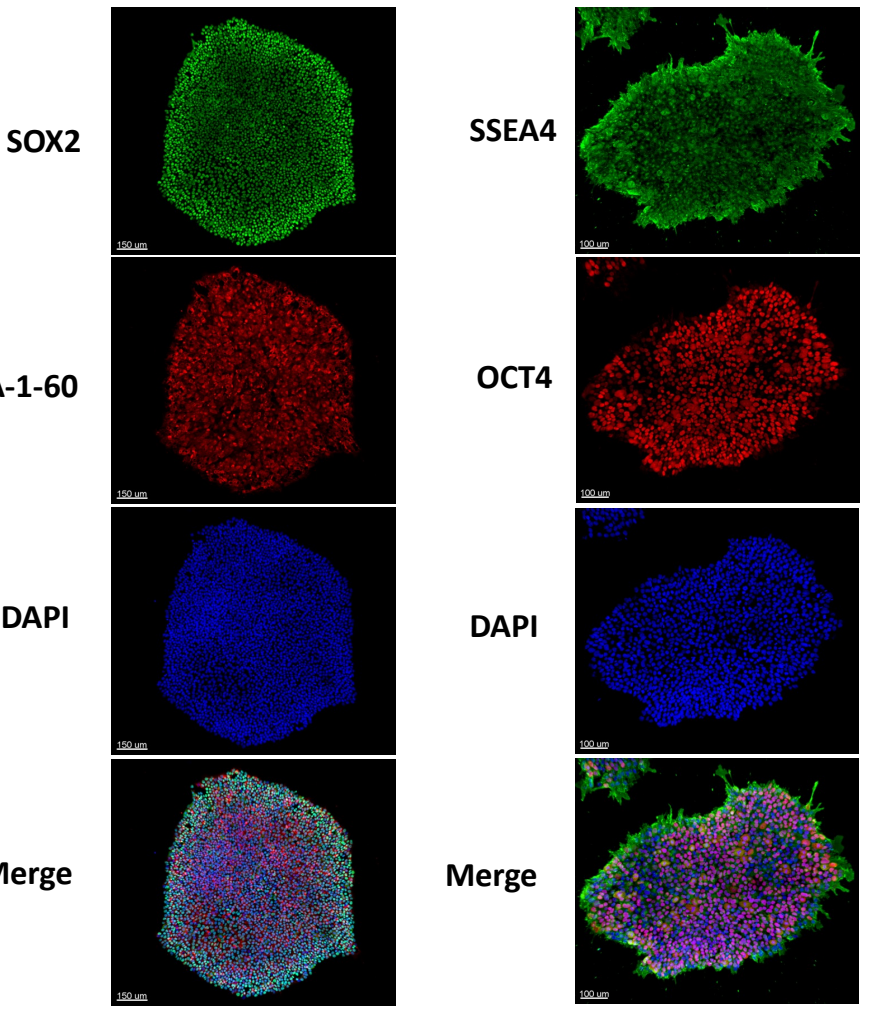

E

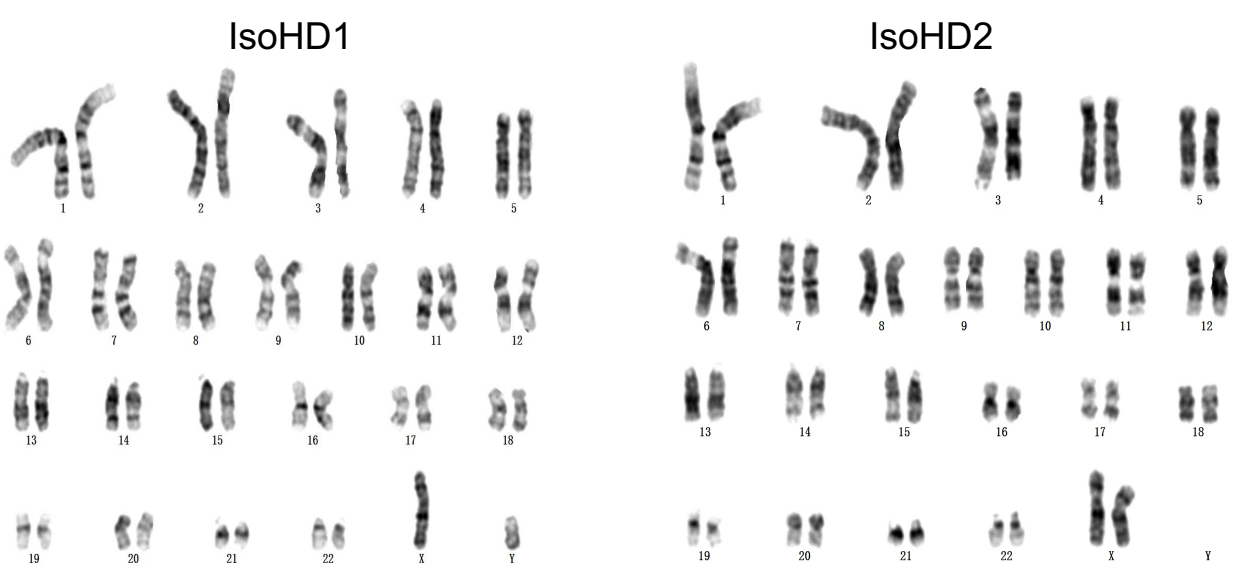

Supp Fig 1

A

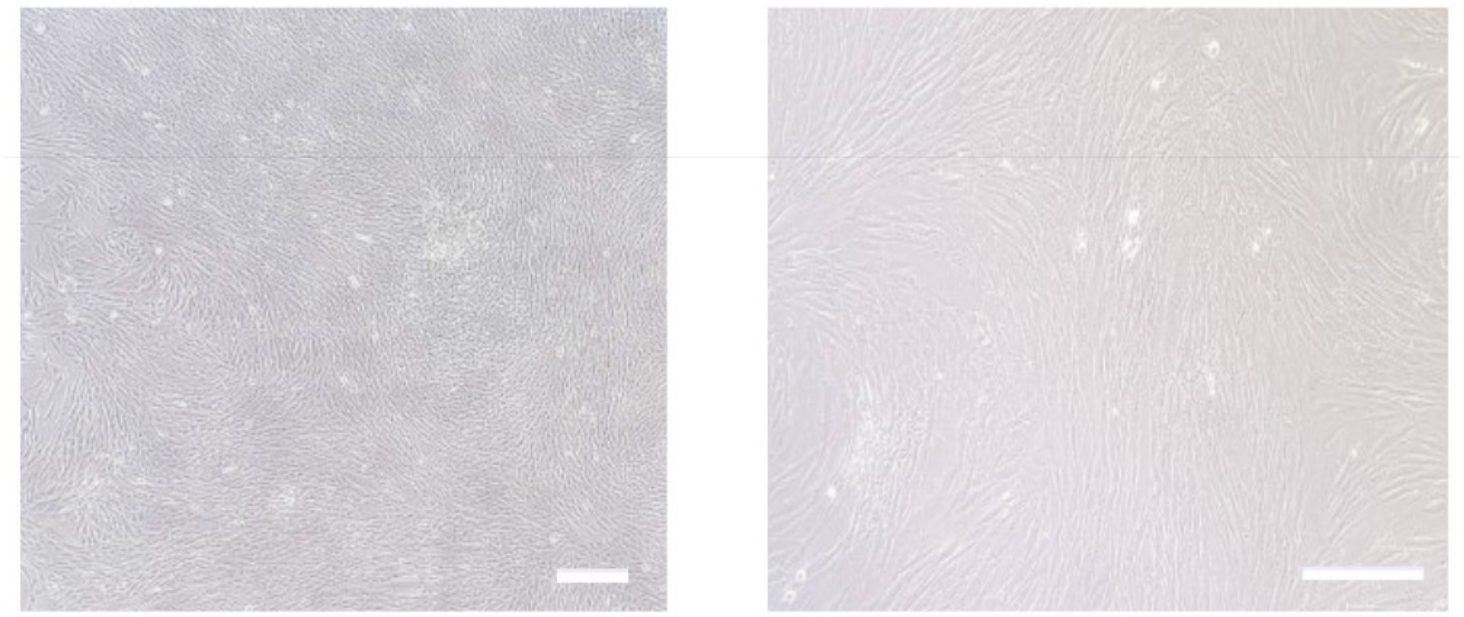

B

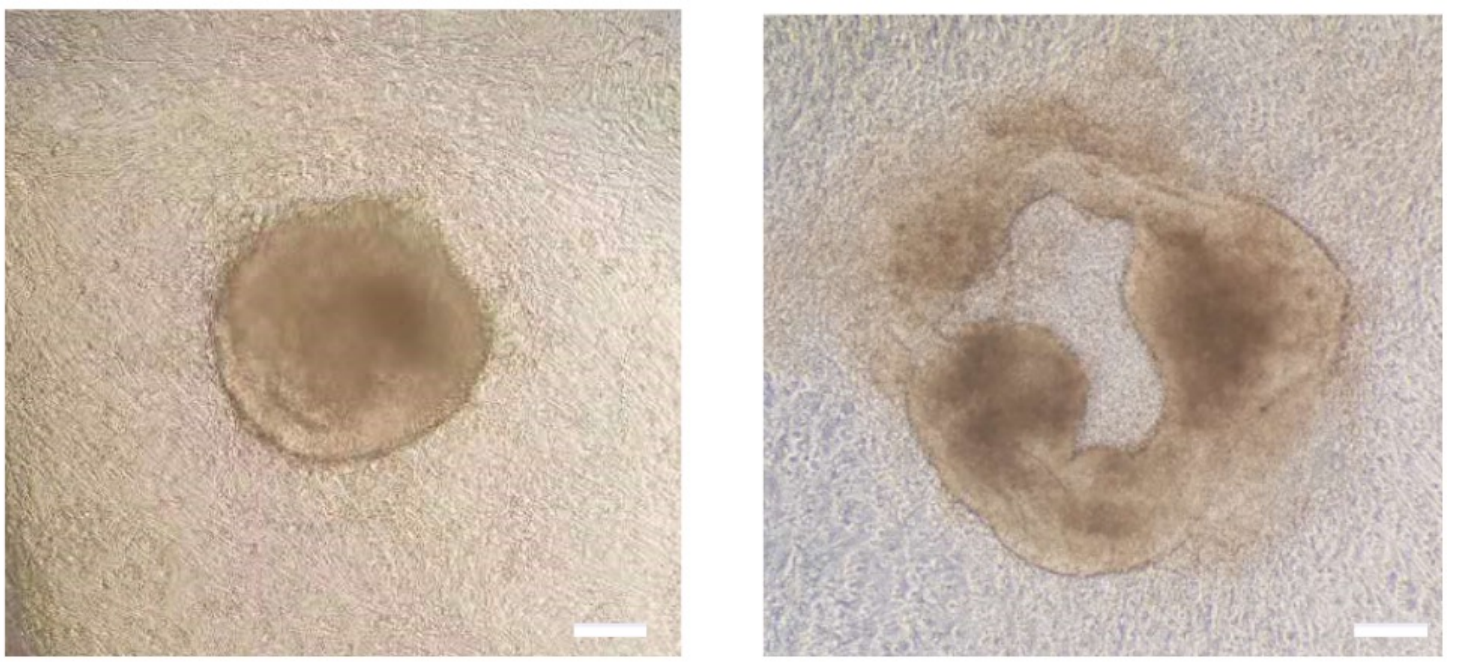

C

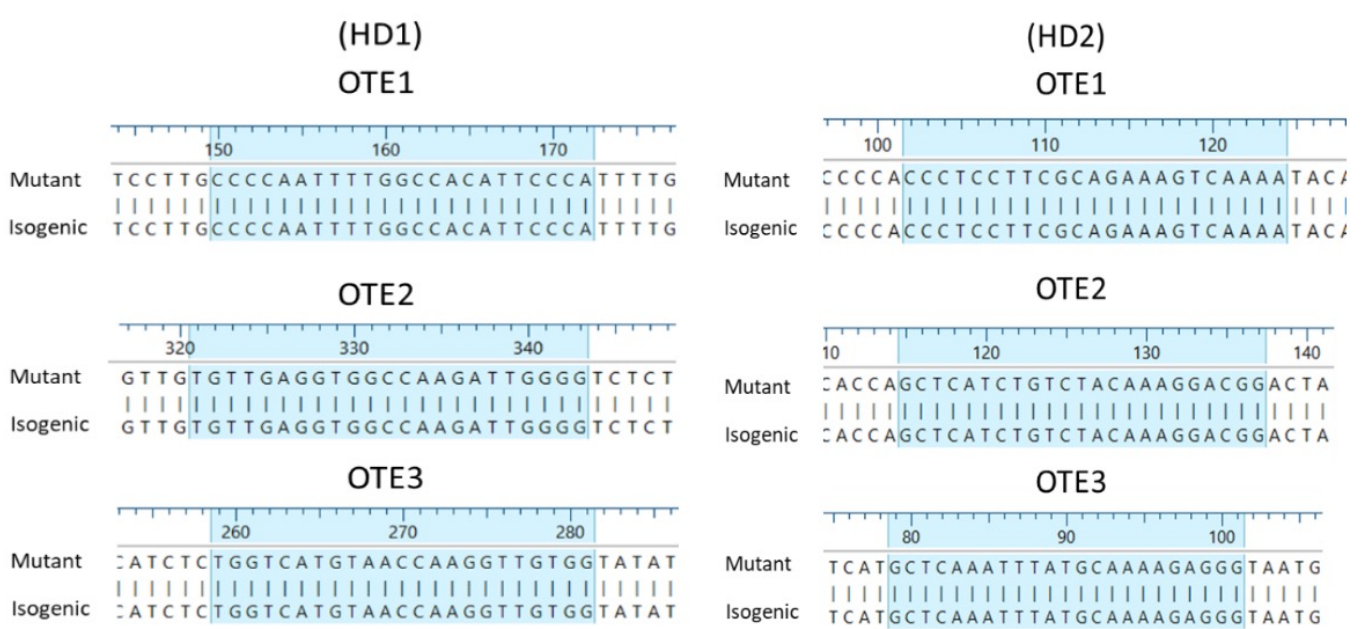

Figure 2

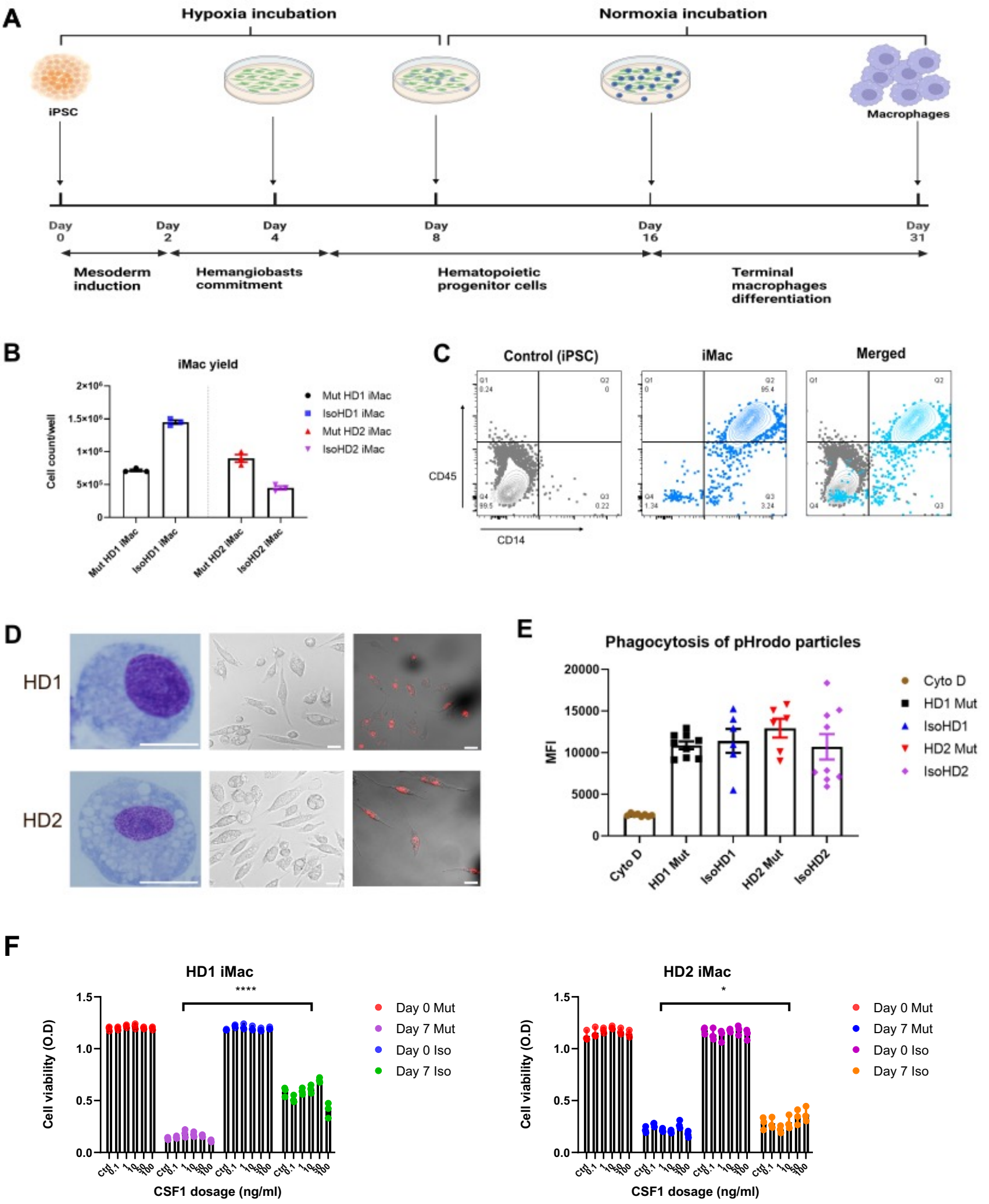
A
Hypoxia incubation
Normoxia incubation
iPSC
Macrophages
Day 0
Day 2
Day 4
Day 8
Day 16
Day 31
Mesoderm induction
Hemangiobasts commitment
Hematopoietic progenitor cells
Terminal macrophages differentiation
B
iMac yield
Cell count/well
Mut HD1 iMac
IsoHD1 iMac
Mut HD2 iMac
IsoHD2 iMac
C
Control (iPSC)
iMac
Merged
CD45
CD14
D
HD1
HD2
E
Phagocytosis of pHrodo particles
MFI
Cyto D
HD1 Mut
IsoHD1
HD2 Mut
IsoHD2
F
HD1 iMac
HD2 iMac
Cell viability (O.D)
CSF1 dosage (ng/ml)
Day 0 Mut
Day 7 Mut
Day 0 Iso
Day 7 Iso

Figure 3

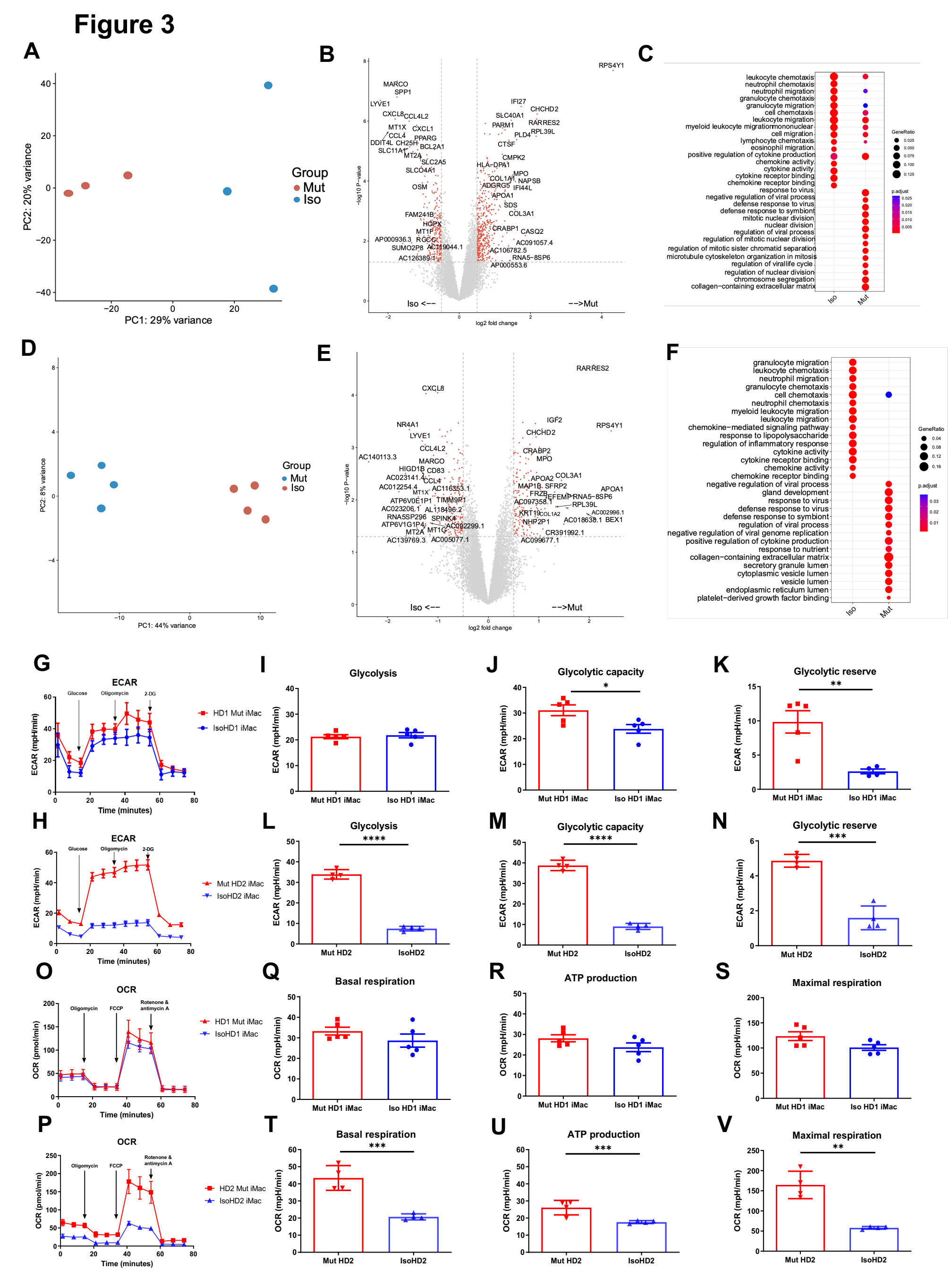
A
PC2: 20% variance
PC1: 29% variance
Group
Mut
Iso
B
RPS4Y1
MARCO
SPP1
LYVE1
CXCL8
CCL4L2
MT1X
CXCL1
CCL4
PPARG
DDIT4L
CH25H
SLC11A1
BCL2A1
MT2A
SLC2A5
SLCO4A1
OSM
FAM241B
HOPX
MT1F
AP000936.3
RGCC
SUMO2P8
AC119044.1
AC126389.1
IFI27
CHCHD2
SLC40A1
PARM1
RARRES2
RPL39L
PLD4
CTSF
CMPK2
HLA-DPA1
MPO
COL1A1
NAPSB
ADGRG5
IFI44L
APOA1
SDS
COL3A1
CRABP1
CASQ2
AC091057.4
AC106782.5
RNA5-8SP6
AP000553.6
Iso <--
-->Mut
-log10 P-value
log2 fold change
C
leukocyte chemotaxis
neutrophil chemotaxis
neutrophil migration
granulocyte chemotaxis
granulocyte migration
cell chemotaxis
leukocyte migration
myeloid leukocyte migration
mononuclear cell migration
lymphocyte chemotaxis
eosinophil migration
positive regulation of cytokine production
chemokine activity
cytokine activity
cytokine receptor binding
chemokine receptor binding
response to virus
negative regulation of viral process
defense response to virus
defense response to symbiont
mitotic nuclear division
nuclear division
regulation of viral process
regulation of mitotic nuclear division
regulation of mitotic sister chromatid separation
microtubule cytoskeleton organization in mitosis
regulation of virallife cycle
regulation of nuclear division
chromosome segregation
collagen-containing extracellular matrix
Iso
Mut
GeneRatio
p.adjust
D
PC2: 8% variance
PC1: 44% variance
Group
Mut
Iso
E
RARRES2
CXCL8
NR4A1
LYVE1
CCL4L2
AC140113.3
MARCO
HIGD1B
CD83
AC023141.4
CCL4
AC012254.4
MT1X
AC116353.1
ATP6V0E1P1
TIMM9P1
AC023206.1
AL118496.2
RNA5SP296
SPINK4
ATP6V1G1P4
AC092299.1
MT2A
MT1G
AC139769.3
AC005077.1
IGF2
RPS4Y1
CHCHD2
CRABP2
MPO
APOA2
COL3A1
MAP1B
SFRP2
APOA1
FRZB
EFEMP1
RNA5-8SP6
AC097358.1
RPL39L
KRT19
COL1A2
AC002996.1
NHP2P1
AC018638.1
BEX1
CR391992.1
AC099677.1
Iso <--
-->Mut
-log10 P-value
log2 fold change
F
granulocyte migration
leukocyte chemotaxis
neutrophil migration
granulocyte chemotaxis
cell chemotaxis
neutrophil chemotaxis
myeloid leukocyte migration
leukocyte migration
chemokine-mediated signaling pathway
response to lipopolysaccharide
regulation of inflammatory response
cytokine activity
cytokine receptor binding
chemokine activity
chemokine receptor binding
negative regulation of viral process
gland development
response to virus
defense response to virus
defense response to symbiont
regulation of viral process
negative regulation of viral genome replication
positive regulation of cytokine production
response to nutrient
collagen-containing extracellular matrix
secretory granule lumen
cytoplasmic vesicle lumen
vesicle lumen
endoplasmic reticulum lumen
platelet-derived growth factor binding
Iso
Mut
GeneRatio
p.adjust
G
ECAR
Glucose
Oligomycin
2-DG
ECAR (mpH/min)
Time (minutes)
HD1 Mut iMac
IsoHD1 iMac
H
ECAR
Glucose
Oligomycin
2-DG
ECAR (mpH/min)
Time (minutes)
Mut HD2 iMac
IsoHD2 iMac
O
OCR
Oligomycin
FCCP
Rotenone & antimycin A
OCR (pmol/min)
Time (minutes)
HD1 Mut iMac
IsoHD1 iMac
P
OCR
Oligomycin
FCCP
Rotenone & antimycin A
OCR (pmol/min)
Time (minutes)
HD2 Mut iMac
IsoHD2 iMac
I
Glycolysis
ECAR (mpH/min)
Mut HD1 iMac
Iso HD1 iMac
J
Glycolytic capacity
*
ECAR (mpH/min)
Mut HD1 iMac
Iso HD1 iMac
K
Glycolytic reserve
**
ECAR (mpH/min)
Mut HD1 iMac
Iso HD1 iMac
L
Glycolysis
****
ECAR (mpH/min)
Mut HD2
IsoHD2
M
Glycolytic capacity
****
ECAR (mpH/min)
Mut HD2
IsoHD2
N
Glycolytic reserve
***
ECAR (mpH/min)
Mut HD2
IsoHD2
Q
Basal respiration
OCR (mpH/min)
Mut HD1 iMac
Iso HD1 iMac
R
ATP production
OCR (mpH/min)
Mut HD1 iMac
Iso HD1 iMac
S
Maximal respiration
OCR (mpH/min)
Mut HD1 iMac
Iso HD1 iMac
T
Basal respiration
***
OCR (mpH/min)
Mut HD2
IsoHD2
U
ATP production
***
OCR (mpH/min)
Mut HD2
IsoHD2
V
Maximal respiration
**
OCR (mpH/min)
Mut HD2
IsoHD2

Figure 4

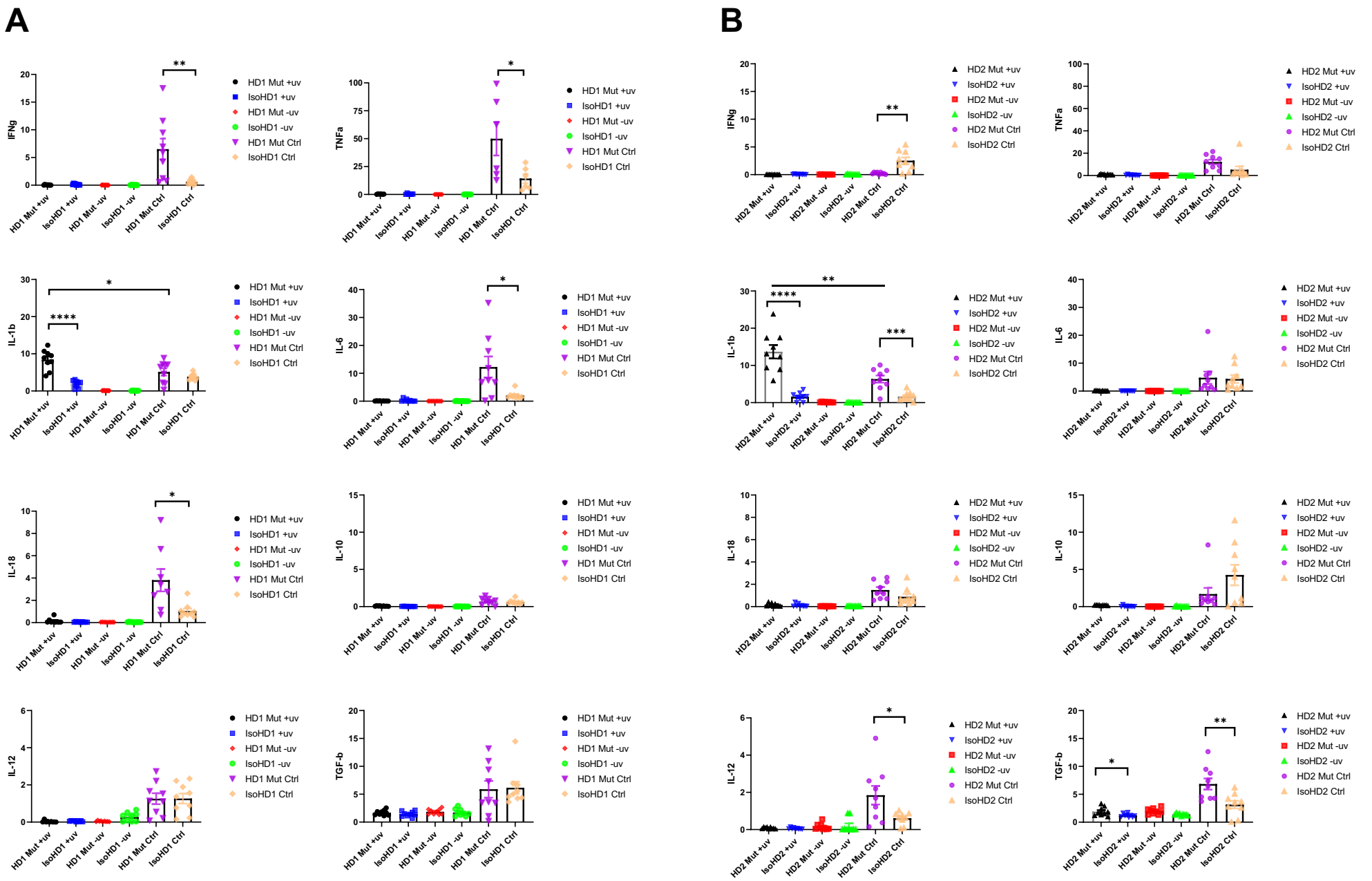
A
B
IFNg
TNFa
IL-1b
IL-6
IL-18
IL-10
IL-12
TGF-b
HD1 Mut +uv
IsoHD1 +uv
HD1 Mut -uv
IsoHD1 -uv
HD1 Mut Ctrl
IsoHD1 Ctrl
HD2 Mut +uv
IsoHD2 +uv
HD2 Mut -uv
IsoHD2 -uv
HD2 Mut Ctrl
IsoHD2 Ctrl

Supp Fig 2

A

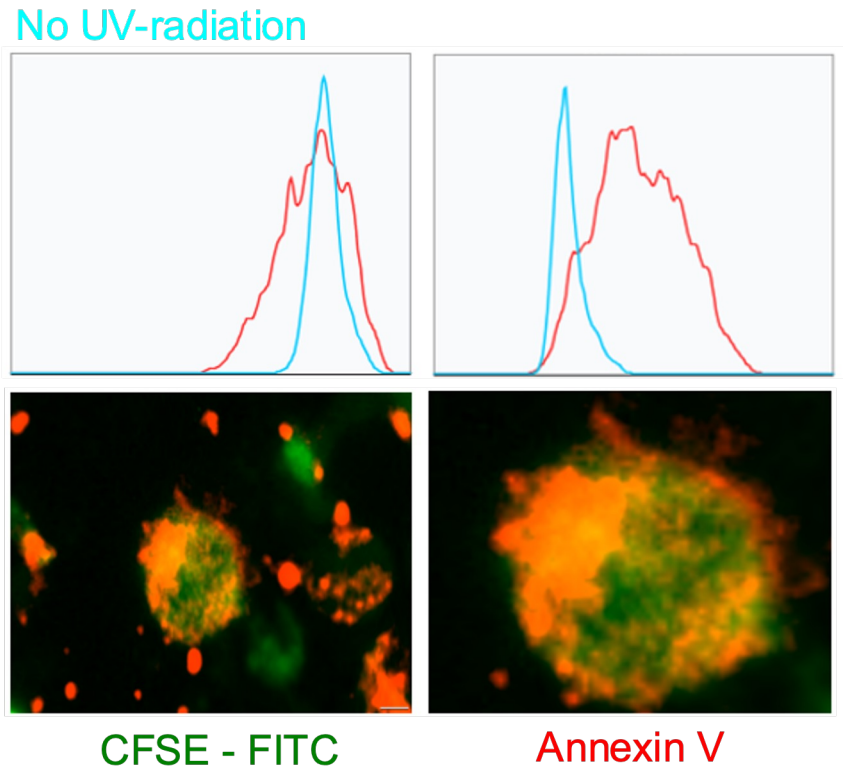
UV-radiation
No UV-radiation
CFSE - FITC
Annexin V

B

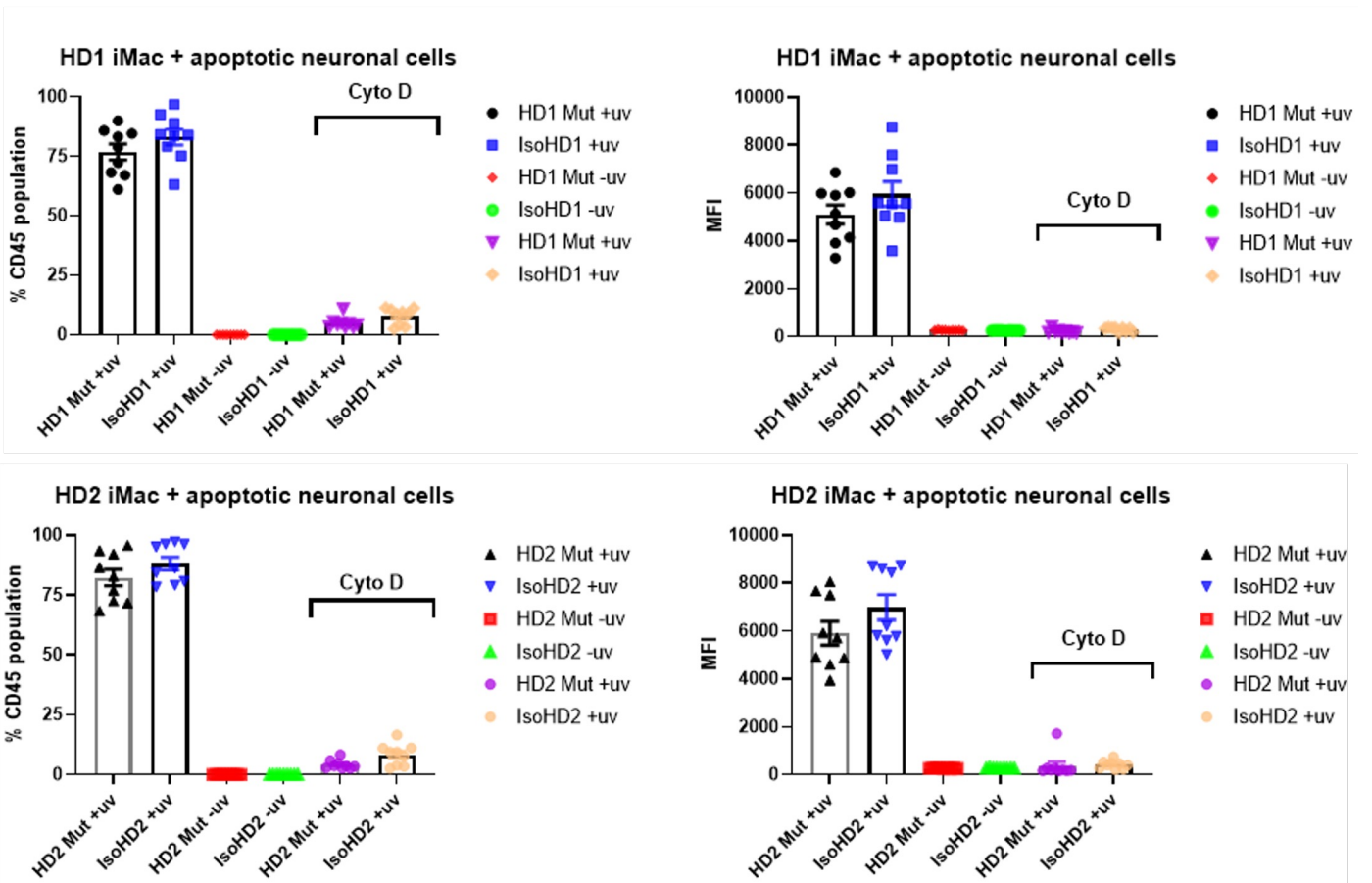
HD1 iMac + apoptotic neuronal cells
% CD45 population
Cyto D
HD1 Mut +uv
IsoHD1 +uv
HD1 Mut -uv
IsoHD1 -uv
HD1 Mut +uv
IsoHD1 +uv
HD1 iMac + apoptotic neuronal cells
MFI
Cyto D
HD1 Mut +uv
IsoHD1 +uv
HD1 Mut -uv
IsoHD1 -uv
HD1 Mut +uv
IsoHD1 +uv
HD2 iMac + apoptotic neuronal cells
% CD45 population
Cyto D
HD2 Mut +uv
IsoHD2 +uv
HD2 Mut -uv
IsoHD2 -uv
HD2 Mut +uv
IsoHD2 +uv
HD2 iMac + apoptotic neuronal cells
MFI
Cyto D
HD2 Mut +uv
IsoHD2 +uv
HD2 Mut -uv
IsoHD2 -uv
HD2 Mut +uv
IsoHD2 +uv

Figure 5

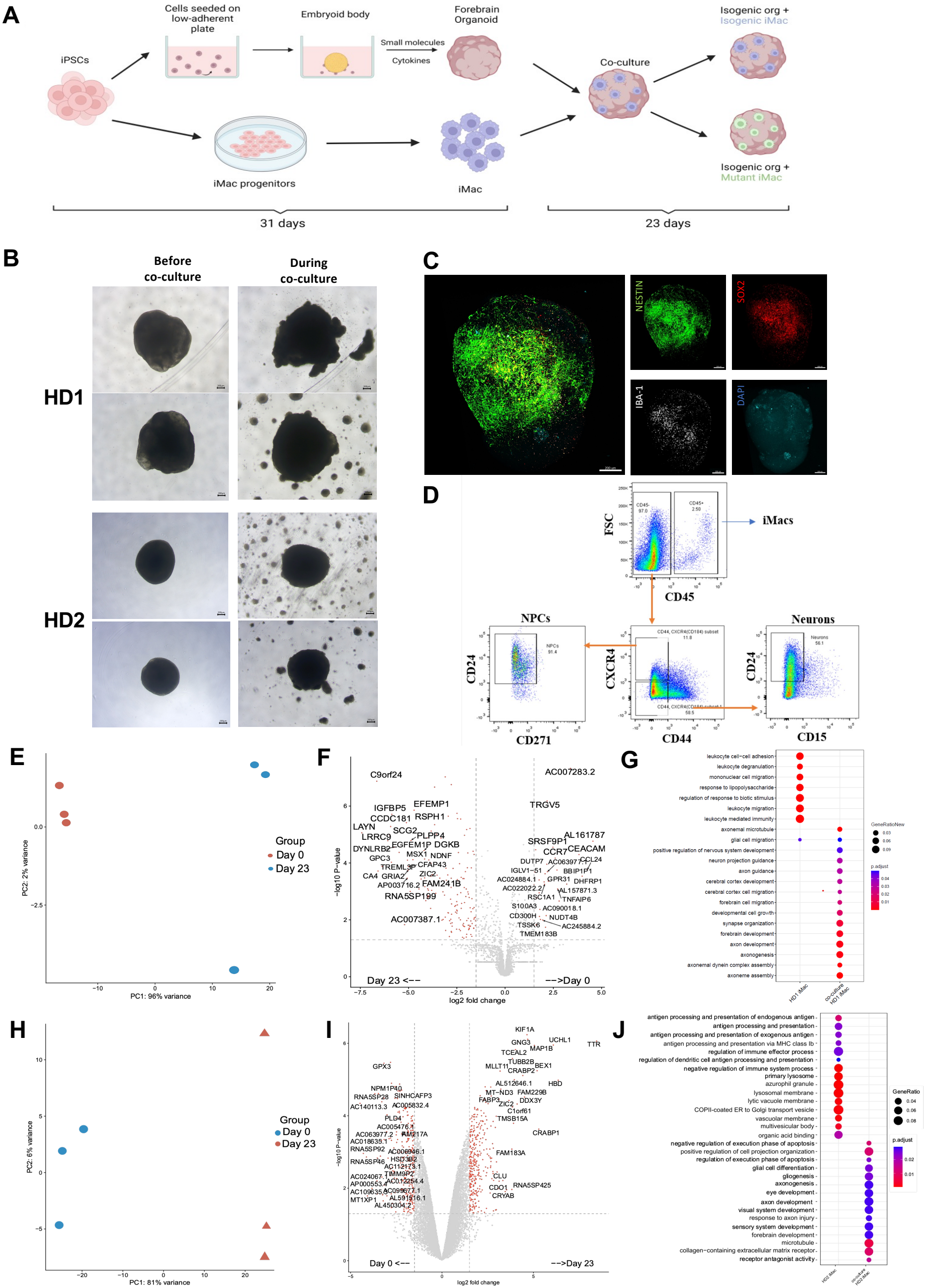
A
iPSCs
Cells seeded on low-adherent plate
Embryoid body
Small molecules
Cytokines
Forebrain Organoid
iMac progenitors
iMac
Co-culture
Isogenic org + Isogenic iMac
Isogenic org + Mutant iMac
31 days
23 days
B
Before co-culture
During co-culture
HD1
HD2
C
NESTIN
SOX2
IBA-1
DAPI
D
FSC
CD45
iMacs
NPCs
CD24
CD271
CXCR4
CD44
Neurons
CD15
E
PC2: 2% variance
PC1: 96% variance
Group
Day 0
Day 23
F
C9orf24
AC007283.2
IGFBP5
EFEMP1
TRGV5
CCDC181
RSPH1
LAYN
SCG2
LRRC9
PLPP4
SRSF9P1
AL161787
DYNLRB2
EGFEM1P
DGKB
CCR7
CEACAM
GPC3
MSX1
NDNF
DUTP7
AC063977.1
CCL24
TREML3P
CFAP43
IGLV1-51
BBIP1P1
CA4
GRIA2
ZIC2
AC024884.1
GPR31
DHFRP1
AP003716.2
FAM241B
AC022022.2
AL157871.3
RNA5SP199
RSC1A1
TNFAIP6
S100A3
AC090018.1
AC007387.1
CD300H
NUDT4B
TSSK6
AC245884.2
TMEM183B
Day 23 <--
-->Day 0
-log10 P-value
log2 fold change
G
leukocyte cell-cell adhesion
leukocyte degranulation
mononuclear cell migration
response to lipopolysaccharide
regulation of response to biotic stimulus
leukocyte migration
leukocyte mediated immunity
axonemal microtubule
glial cell migration
positive regulation of nervous system development
neuron projection guidance
axon guidance
cerebral cortex development
cerebral cortex cell migration
forebrain cell migration
developmental cell growth
synapse organization
forebrain development
axon development
axonogenesis
axonemal dynein complex assembly
axoneme assembly
HD1 iMac
co-culture HD1 iMac
GeneRatioNew
p.adjust
H
PC2: 6% variance
PC1: 81% variance
Group
Day 0
Day 23
I
KIF1A
GNG3
UCHL1
TTR
MAP1B
TCEAL2
TUBB2B
MLLT11
BEX1
GPX3
CRABP2
AL512646.1
HBD
NPM1P40
MT-ND3
FAM229B
RNA5SP28
SINHCAFP3
FABP3
DDX3Y
AC140113.3
AC005832.4
ZIC2
C1orf61
PLD4
TMSB15A
AC005476.1
AC063977.2
FAM217A
CRABP1
AC018635.1
RNA5SP92
AC006946.1
FAM183A
RNA5SP46
HSD3B2
AC112173.1
TIMM9P2
CLU
AC024067.1
AC012254.4
AP000553.4
CDO1
RNA5SP425
AC109635.3
AC099677.1
CRYAB
MT1XP1
AL591516.1
AL450304.2
Day 0 <--
-->Day 23
-log10 P-value
log2 fold change
J
antigen processing and presentation of endogenous antigen
antigen processing and presentation
antigen processing and presentation of exogenous antigen
antigen processing and presentation via MHC class Ib
regulation of immune effector process
regulation of dendritic cell antigen processing and presentation
negative regulation of immune system process
primary lysosome
azurophil granule
lysosomal membrane
lytic vacuole membrane
COPII-coated ER to Golgi transport vesicle
vascuolar membrane
multivesicular body
organic acid binding
negative regulation of execution phase of apoptosis
positive regulation of cell projection organization
regulation of execution phase of apoptosis
glial cell differentiation
gliogenesis
axonogenesis
eye development
axon development
visual system development
response to axon injury
sensory system development
forebrain development
microtubule
collagen-containing extracellular matrix receptor
receptor antagonist activity
HD2 iMac
co-culture HD2 iMac
GeneRatio
p.adjust

Supp Fig 3

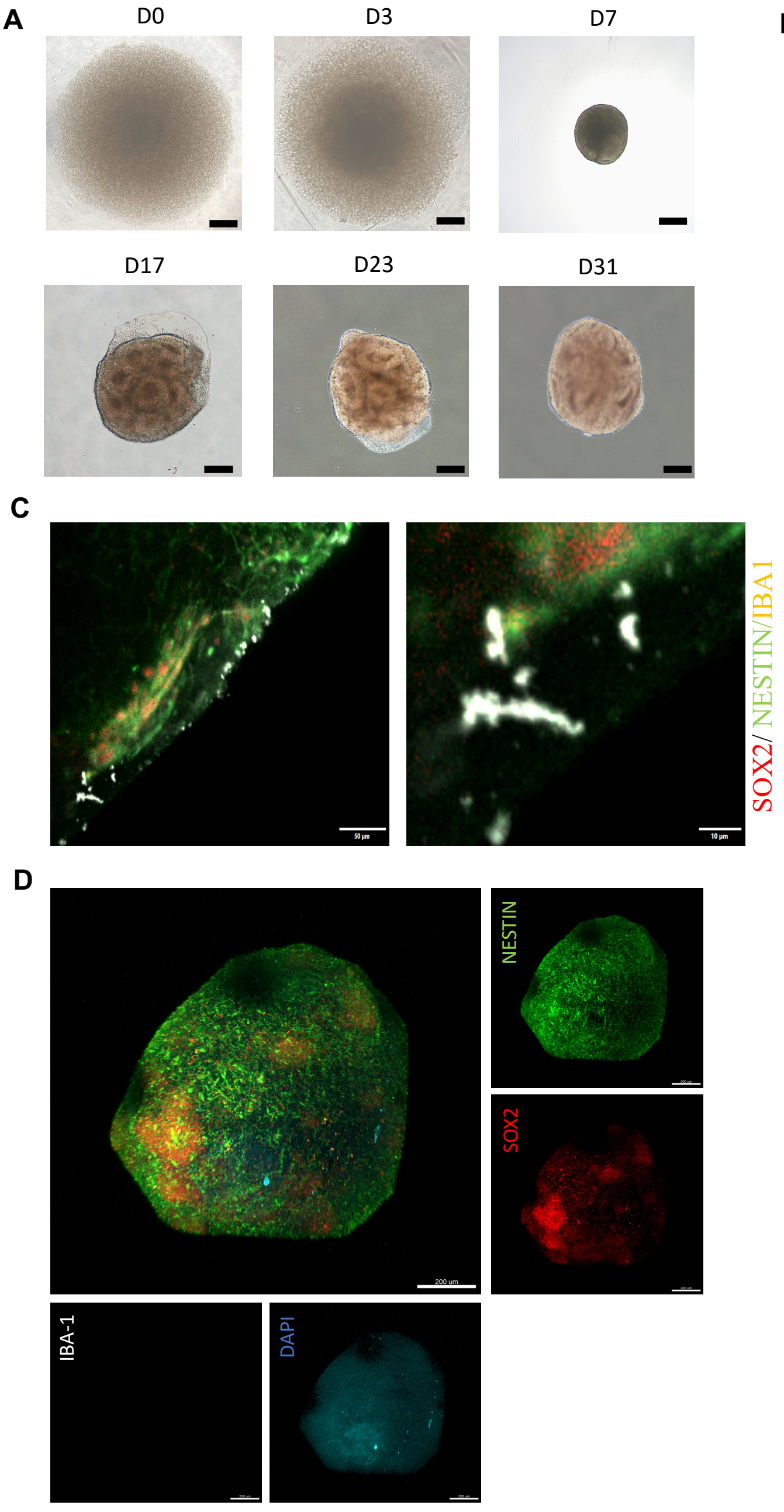
A
D0
D3
D7
D17
D23
D31
B
SOX2/ NESTIN
C
SOX2/ NESTIN/IBA1
50 µm
10 µm
D
NESTIN
SOX2
IBA-1
DAPI
200 um

Figure 6

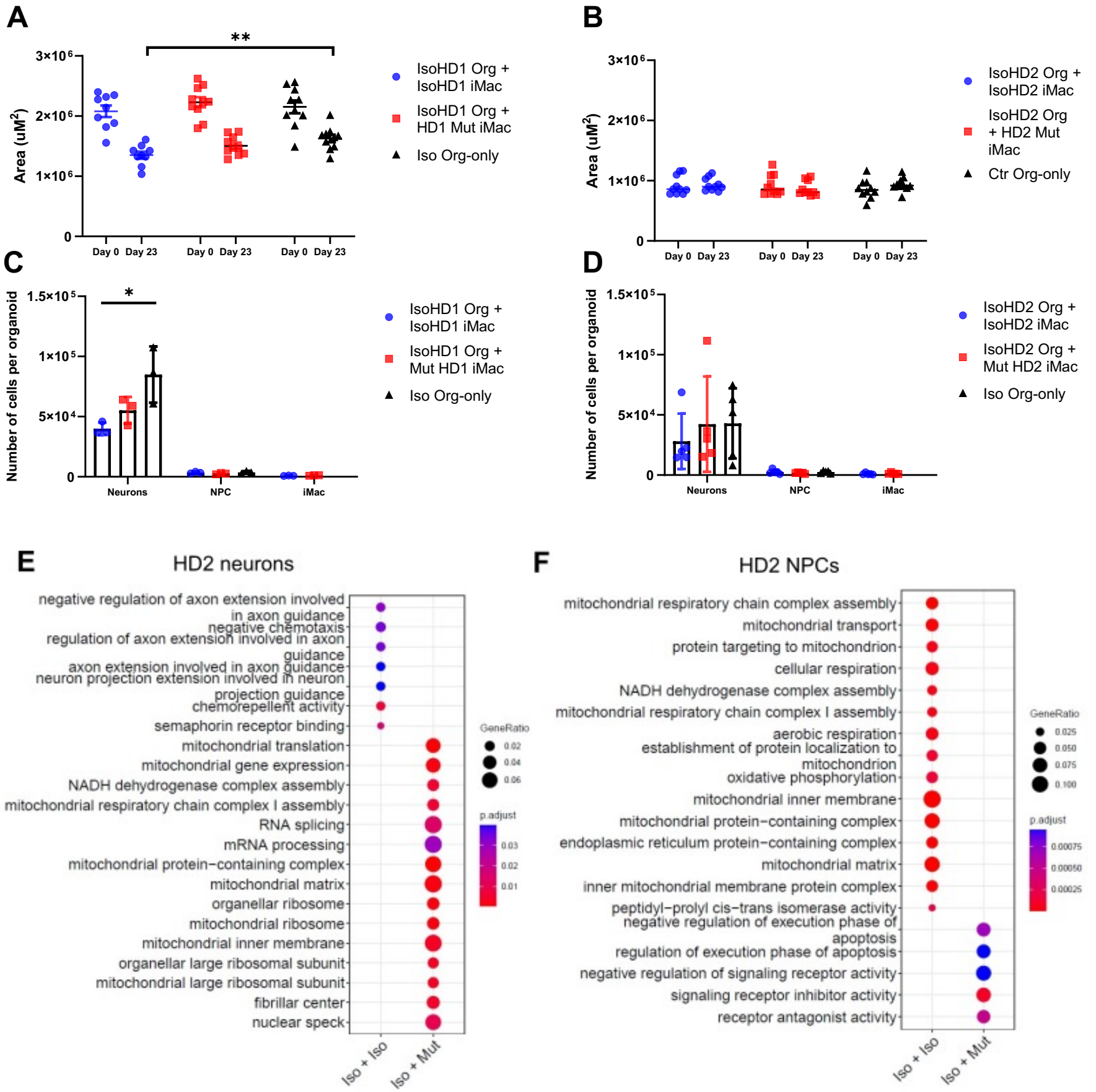
A
**
Area (uM²)
3×10⁶
2×10⁶
1×10⁶
0
Day 0 Day 23 Day 0 Day 23 Day 0 Day 23
IsoHD1 Org + IsoHD1 iMac
IsoHD1 Org + HD1 Mut iMac
Iso Org-only
B
Area (uM²)
3×10⁶
2×10⁶
1×10⁶
0
Day 0 Day 23 Day 0 Day 23 Day 0 Day 23
IsoHD2 Org + IsoHD2 iMac
IsoHD2 Org + HD2 Mut iMac
Ctr Org-only
C
*
Number of cells per organoid
1.5×10⁵
1×10⁵
5×10⁴
0
Neurons NPC iMac
IsoHD1 Org + IsoHD1 iMac
IsoHD1 Org + Mut HD1 iMac
Iso Org-only
D
Number of cells per organoid
1.5×10⁵
1×10⁵
5×10⁴
0
Neurons NPC iMac
IsoHD2 Org + IsoHD2 iMac
IsoHD2 Org + Mut HD2 iMac
Iso Org-only
E
HD2 neurons
negative regulation of axon extension involved in axon guidance
negative chemotaxis
regulation of axon extension involved in axon guidance
axon extension involved in axon guidance
neuron projection extension involved in neuron projection guidance
chemorepellent activity
semaphorin receptor binding
mitochondrial translation
mitochondrial gene expression
NADH dehydrogenase complex assembly
mitochondrial respiratory chain complex I assembly
RNA splicing
mRNA processing
mitochondrial protein−containing complex
mitochondrial matrix
organellar ribosome
mitochondrial ribosome
mitochondrial inner membrane
organellar large ribosomal subunit
mitochondrial large ribosomal subunit
fibrillar center
nuclear speck
Iso + Iso
Iso + Mut
GeneRatio
0.02
0.04
0.06
p.adjust
0.03
0.02
0.01
F
HD2 NPCs
mitochondrial respiratory chain complex assembly
mitochondrial transport
protein targeting to mitochondrion
cellular respiration
NADH dehydrogenase complex assembly
mitochondrial respiratory chain complex I assembly
aerobic respiration
establishment of protein localization to mitochondrion
oxidative phosphorylation
mitochondrial inner membrane
mitochondrial protein−containing complex
endoplasmic reticulum protein−containing complex
mitochondrial matrix
inner mitochondrial membrane protein complex
peptidyl−prolyl cis−trans isomerase activity
negative regulation of execution phase of apoptosis
regulation of execution phase of apoptosis
negative regulation of signaling receptor activity
signaling receptor inhibitor activity
receptor antagonist activity
Iso + Iso
Iso + Mut
GeneRatio
0.025
0.050
0.075
0.100
p.adjust
0.00075
0.00050
0.00025